TAMPERE UNIVERSITY OF TECHNOLOGY

Research Article

Efficient Delay Tracking Methods with Sidelobes Cancellation for BOC-Modulated Signals

Adina Burian, Elena Simona Lohan, and Markku Kalevi Renfors

Institute of Communications Engineering, Tampere University of Technology, P.O. Box 553, 33101 Tampere, Finland

In positioning applications, where the line of sight (LOS) is needed with high accuracy, the accurate delay estimation is an important task. The new satellite-based positioning systems, such as Galileo and modernized GPS, will use a new modulation type, that is, the binary offset carrier (BOC) modulation. This type of modulation creates multiple peaks (ambiguities) in the envelope of the correlation function, and thus triggers new challenges in the delay-frequency acquisition and tracking stages. Moreover, the properties of BOC-modulated signals are yet not well studied in the context of fading multipath channels. In this paper, sidelobe cancellation techniques are applied with various tracking structures in order to remove or diminish the side peaks, while keeping a sharp and narrow main lobe, thus allowing a better tracking. Five sidelobe cancellation methods (SCM) are proposed and studied: SCM with interference cancellation (IC), SCM with narrow correlator, SCM with high-resolution correlator (HRC), SCM with differential correlation (DC), and SCM with threshold. Compared to other delay tracking methods, the proposed SCM approaches have the advantage that they can be applied to any sine or cosine BOC-modulated signal. We analyze the performances of various tracking techniques in the presence of fading multipath channels and we compare them with other methods existing in the literature. The SCM approaches bring improvement also in scenarios with closely-spaced paths, which are the most problematic from the accurate positioning point of view.

1. INTRODUCTION

Applications of new generations of Global Navigation Satellite Systems (GNSS) are developing rapidly and attract a great interest. The modernized GPS proposals have been recently defined [1, 2] and the first version of Galileo (the new European Satellite System) standards has been released in May 2006 [3]. Both GPS and Galileo signals use direct sequence-code division multiple access (DS-CDMA) technology, where code and frequency synchronizations are important stages at the receiver. The GNSS receivers estimate jointly the code phase and the Doppler spreads through a two-dimensional searching process in time-frequency plane. This delay-Doppler estimation process is done in two phases, first a coarse estimation stage (acquisition), followed by the fine estimation stage (tracking). The mobile wireless channels suffer adverse effects during transmission, such as presence of multipath propagation, high level of noise, or obstruction of LOS by one or several closely spaced non-LOS components (especially in indoor environments). The fading of channel paths induces a certain Doppler spread, related

to the terminal speed. Also, the satellite movement induces a Doppler shift, which deteriorates the performance, if not correctly estimated and removed [4].

Since both the GPS and Galileo systems will send several signals on the same carriers, a new modulation type has been selected. This binary offset carrier (BOC) modulation has been proposed in [5], in order to get a more efficient sharing of the L-band spectrum by multiple civilian and military users. The spectral efficiency is obtained by moving the signal energy away from the band center, thus achieving a higher degree of spectral separation between the BOC-modulated signals and other signals which use the shift-keying modulation, such as the GPS C/A code. The BOC performance has been studied for the GPS military M-signal [6] and later has been also selected for the use with the new Galileo signals [3] and modernized GPS signals. The BOC modulation is a square-wave modulation scheme, which uses the typical non-return-to-zero (NRZ) format [7]. While this type of modulation provides better resistance to multipath and narrowband interference [6], it triggers new challenges in the delay estimation process, since deep fades (ambiguities) appear

into the range of the ± 1 chips around the maximum peak of the correlation envelope. Since the receiver can lock on a sidelobe peak, the tracking process has to cope with these false lock points. In conclusion, the acquisition and tracking processes should counteract all these effects, and different methods have been proposed in literature, in order to alleviate multipath propagation and/or side-peaks ambiguities.

In order to minimize the influence of multipath errors, which are the dominating error sources for many GNSS applications, several receiver-internal correlation approaches have been proposed. During the 1990's, a variety of receiver architectures were introduced in order to mitigate the multipath for GPS C/A code or GLONASS. The traditional GPS receiver employs a delay-lock loop (DLL) with a spacing Δ between the early and late correlators of one chip. However, due to presence of multipath, this wide DLL, which should track the incoming signal within the receiver, is not able to align perfectly the local code with the incoming signal, since the presence of multipath (within a delay of 1.5 chips) creates a bias of the zero-crossing point of the S-curve function. A first approach to reduce the influences of code multipath is the narrow correlator or narrow early minus-late (NEML) tracking loop introduced for GPS receivers by NovAtel [8]. Instead of using a standard (wide) correlator, the chip spacing of a narrow correlator is less than one chip (typically $\Delta = 0.1$ chips). The lower bound on the correlator spacing depends on the available bandwidth. Correlator spacings of $\Delta = 0.1$ and $\Delta = 0.05$ chips are commercially available for GPS.

Another family of tracking loops proposed for GPS are the so-called double-delta ($\Delta\Delta$) correlators, which are the general name for special code discriminators which are formed by two correlator pairs instead of one [9]. Some well-known implementations of $\Delta\Delta$ concept are the high-resolution correlator (HRC) [10], the Ashtech's Strobe Correlator [11], or the NovAtel's Pulse Aperture Correlator [12]. Another similar tracking method with $\Delta\Delta$ structure is the Early1/Early2 tracking [13], where two correlators are located on the early slope of the correlation function (with an arbitrary spacing); their amplitudes are compared with the amplitudes of an ideal reference correlation function and based on the measured amplitudes and reference amplitudes, a delay correction factor is calculated. The Early1/Early2 tracker shows the worst multipath performance for short- and medium-delay multipath compared to the HRC or the Strobe Correlator [9].

The early late slope technique [9], also called Multipath Elimination Technology, is based on determining the slope at both sides of autocorrelation function's central peak. Once both slopes are known, they can be used to perform a pseudorange correction. Simulation results showed that in multipath environments, the early late slope technique is outperformed by HRC and Strobe correlators [9]. Also, it should be mentioned that in cases of Narrow Correlator, $\Delta\Delta$, early-late slope, or Early1/Early2 methods the BOC(n,n) modulated signal outperforms the BPSK modulated signals, for multipath delays greater than approximately 0.5 chips (long-delay multipath) [9]. A scheme based on the slope differential of the correlation function has been proposed in [14].

This scheme employs only the prompt correlator and in presence of multipath, it has an unbiased tracking error, unlike the narrow or strobe correlators schemes, which have a biased tracking error due to the nonsymmetric property of the correlation output. However, the performance measure was solely based on the multipath error envelope curves, thus its potential in more realistic multipath environments is still an open issue. One algorithm proposed to diminish the effect of multipath for GPS application is the multipath estimating delay locked loop (MEDLL) [15]. This method is different in that it is not based on a discriminator function, but instead forms estimates of delay and phase of direct LOS signal component and of the indirect multipath components. It uses a reference correlation function in order to determine the best combinations of LOS and NLOS components (i.e., amplitudes, delays, phases, and number of multipaths) which would have produced the measured correlation function.

As mentioned above, in the case of BOC-modulated signals, besides the multipath propagation problem, the sidelobes peaks ambiguities should be also taken into account. In order to counteract this issue, different approaches have been introduced. One method considered in [16] is the partial Sideband discriminator, which uses weighted combinations of the upper and lower sidebands of received signal, to obtain modified upper and lower signals. A "bump-jumping" algorithm is presented in [17]. The "bump-jumping" discriminator tracks the ambiguous offset that arises due to multi-peaked Autocorrelation Function (ACF), making amplitude comparisons of the prompt peak with those of neighboring peaks, but it does not resolve continuously the ambiguity issue. An alternative method of preventing incorrect code tracking is proposed in [18]. This technique relies on summation of two different discriminator S-curves (named here restoring forces), derived from coherent, respectively noncoherent combining of the sidebands. One drawback is that there is a noise penalty which increases as carrier-to-noise ratio (CNR) decreases, but it does not seem excessive [18]. A new approach which design a new replica code and produces a continuously unambiguous BOC correlation is described in [19].

The methods proposed in [16–19] tend to destroy the sharp peak of the ACF, while removing its ambiguities. However, for accurate delay tracking, preserving a sharp peak of the ACF is a prerequisite. An innovative unambiguous tracking technique, that keeps the sharp correlation of the main peak, is proposed in [20]. This approach uses two correlation channels, completely removing the side peaks from the correlation function. However, this method is verified for the particular case of SinBOC(n,n) modulated signals, and its extension to other sine or cosine BOC signals is not straightforward. A similar method, with a better multipath resistance, is introduced in [21].

Another approach which produces a decrease of sidelobes from ACF is the differential correlation method, where the correlation is performed between two consecutive outputs of coherent integration [22].

In this paper, we analyze in details and develop further a novel class of tracking algorithms, introduced by authors in

[23]. These techniques are named the sidelobes cancellation methods (SCM), because they are all based on the idea of suppressing the undesired lobes of the BOC correlation envelope and they cope better with the false lock points (ambiguities) which appear due to BOC modulation, while keeping the sharp shape of the main peak. It can be applied in both acquisition and tracking stages, but due to narrow width of the main peak, only the tracking stage is considered here. In contrast with the approach from [20] (valid only for sine BOC(n, n) cases), our methods have the advantage that they can be generalized to any sine and cosine BOC(m, n) modulation and that they have reduced complexity, since they are based on an ideal reference correlation function, stored at receiver side. In order to deal with both sidelobes ambiguities and multipath problems, we used the sidelobes cancellation idea in conjunction with different discriminators, based on the unambiguous shape of ACF (i.e., the narrow correlator, the high resolution correlator), or after applying the differential correlation method. We also introduced here an SCM method with multipath interference cancellation (SCM IC), where the SCM is used in combination with a MEDLL unit, and also an SCM algorithm based on threshold comparison.

This paper is organized as follows: Section 2 describes the signal model in the presence of BOC modulation. Section 3 presents several representative delay tracking algorithms, employed for comparison with the SCM methods. Section 4 introduces the SCM ideas and presents the SCM usage in conjunction with other delay tracking algorithms or based solely on threshold comparison. The performance evaluation of the new methods with the existing delay estimators, in terms of root mean square error (RMSE) and mean time to lose lock (MTLL), is done in Section 5. The conclusions are drawn in Section 6.

2. SIGNAL MODEL IN PRESENCE OF BOC MODULATION

At the transmitter, the data sequence is first spread and the pseudorandom (PRN) sequence is further BOC-modulated. The BOC modulation is a square subcarrier modulation, where the PRN signal is multiplied by a rectangular subcarrier which has a frequency multiple of code frequency. A BOC-modulated signal (sine or cosine) creates a split spectrum with the two main lobes shifted symmetrically from the carrier frequency by a value of the subcarrier frequency f_{sc} [5].

The usual notation for BOC modulation is BOC(f_{sc}, f_c), where f_c is the chip frequency. For Galileo signals, the BOC(m, n) notation is also used [5], where the sine and cosine BOC modulations are defined via two parameters m and n, satisfying the relationships $m = f_{sc}/f_{ref}$ and $n = f_c/f_{ref}$, where $f_{ref} = 1.023$ MHz is the reference frequency [5, 24]. From the point of view of equivalent baseband signal, BOC modulation can be defined via a single parameter, denoted by the BOC-modulation order $N_{BOC_1} = 2m/n = 2f_{sc}/f_c$. The factor N_{BOC_1} is an integer number [25].

Examples of sine BOC-modulated waveforms for Sin-BOC$(1, 1)$ (even BOC-modulation order $N_{BOC_1} = 2$) and
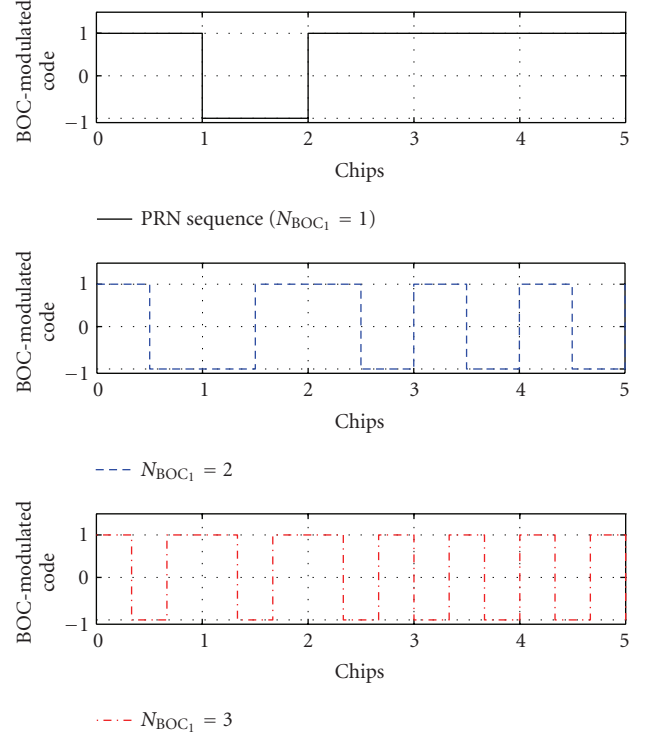

FIGURE 1: Examples of time-domain waveforms for sine BOC-modulated signals.

SinBOC$(15, 10)$ (odd BOC-modulation order $N_{BOC_1} = 3$) together with the original PRN sequence ($N_{BOC_1} = 1$) are shown in Figure 1. In order to consider the cosine BOC-modulation case, a second BOC-modulation order $N_{BOC_2} = 2$ has been defined in [25], in a way that the case of sine BOC-modulation corresponds to $N_{BOC_2} = 1$ and the case of cosine BOC modulation corresponds to $N_{BOC_2} = 2$ (see the expressions of (1) to (4)). After spreading and BOC modulation, the data sequence is oversampled with an oversampled factor of N_s, and this oversampling determines the desired accuracy in the delay estimation process. Thus, the oversampling factor N_s represents the number of samples per BOC interval, and one chip will consists of $N_{BOC_1} N_{BOC_2} N_s$ samples (i.e, the chip period is $T_c = N_s N_{BOC_1} N_{BOC_2} T_s$, where T_s is the sampling rate).

The BOC-modulated signal $s_{n,BOC}(t)$ can be written, in its most general form, as a convolution between a PRN sequence $s_{PRN}(t)$ and a BOC waveform $s_{BOC}(t)$ [25]:

$$s_{n,BOC}(t)$$
$$= \sum_{n=-\infty}^{+\infty} b_n \sum_{k=1}^{S_F} (-1)^{nN_{BOC_1}} c_{k,n} s_{BOC}(t - nT - kT_c)$$
$$= s_{BOC}(t) \otimes \sum_{n=-\infty}^{+\infty} \sum_{k=1}^{S_F} b_n c_{k,n} (-1)^{nN_{BOC_1}} \delta(t - nT - kT_c)$$
$$= s_{BOC}(t) \otimes s_{PRN}(t),$$

$$(1)$$

where b_n is the nth complex data symbol, T is the symbol period (or code epoch length) ($T = S_F T_c$), $c_{k,n}$ is the kth chip corresponding to the nth symbol, $T_c = 1/f_c$ is the chip period, S_F is the spreading factor (i.e., for GPS C/A signal and Galileo OS signal, $S_F = 1023$), $\delta(t)$ is the Dirac pulse, $\otimes$ is the convolution operator and $s_{\mathrm{PRN}}(t)$ is the pseudo-random (PRN) code sequence (including data modulation) of satellite of interest, and $s_{\mathrm{BOC}}(\cdot)$ is the BOC-modulated signal (sine or cosine) whose expression is given in (2) to (4). We remark that the term $(-1)^{nN_{\mathrm{BOC}_1}}$ is included to take into account also odd BOC-modulation orders, similar with [26]. The interference of other satellites is modeled as additive white Gaussian noise, and, for clarity of notations, the continuous-time model is employed here. However, the extension to the discrete-time model is straightforward and all presented results are based on discrete-time implementation.

The SinBOC-CosBOC-modulated waveforms $s_{\mathrm{BOC}}(t)$ are defined as in [5, 25]:

$$s_{\sin/\mathrm{CosBOC}}(t) = \begin{cases} \mathrm{sign}\left(\sin\left(\dfrac{N_{\mathrm{BOC}_1}\pi t}{T_c}\right)\right) & \text{for SinBOC,} \\ \mathrm{sign}\left(\cos\left(\dfrac{N_{\mathrm{BOC}_1}\pi t}{T_c}\right)\right) & \text{for CosBOC,} \end{cases} \tag{2}$$

respectively, that is, for SinBOC-modulation [25],

$$s_{\mathrm{SinBOC}}(t) = \sum_{i=0}^{N_{\mathrm{BOC}_1}-1} (-1)^i p_{T_{B_1}}\left(t - i\frac{T_c}{N_{\mathrm{BOC}}}\right), \tag{3}$$

and for CosBOC-modulation [25],

$$s_{\mathrm{CosBOC}}(t) = \sum_{i=0}^{N_{\mathrm{BOC}_1}-1} \sum_{k=0}^{N_{\mathrm{BOC}_2}-1} (-1)^{i+k} \\ \times p_{T_B}\left(t - i\frac{T_c}{N_{\mathrm{BOC}_1}} - k\frac{T_c}{N_{\mathrm{BOC}_1}N_{\mathrm{BOC}_2}}\right). \tag{4}$$

In (3) and (4), $p_{T_{B_1}}(\cdot)$ is a rectangular pulse of support T_c/N_{BOC_1} and $p_{T_B}(\cdot)$ is a rectangular pulse of support $T_c/N_{\mathrm{BOC}_1}N_{\mathrm{BOC}_2}$. For example,

$$p_{T_B}(t) = \begin{cases} 1 & \text{if } 0 \le t < \dfrac{T_c}{N_{\mathrm{BOC}_1}N_{\mathrm{BOC}_2}}, \\ 0 & \text{otherwise.} \end{cases} \tag{5}$$

We remark that the bandlimiting case can also be taken into account, by setting $p_{T_B}(\cdot)$ to be equal to the pulse shaping filter.

Some examples of the normalized power spectral density (PSD), computed as in [25], for several sine and cosine BOC-modulated signals, are shown in Figure 2. It can be observed that for even-modulation orders such as SinBOC(1, 1) or CosBOC(10, 5) (currently selected or proposed by Galileo Signal Task Force), the spectrum is symmetrically split into two parts, thus moving the signal energy away from DC frequency and thus allowing for less interference with the existing GPS bands (i.e., the BPSK case). Also, it should be mentioned that in case of an odd BOC-modulation order (i.e.,
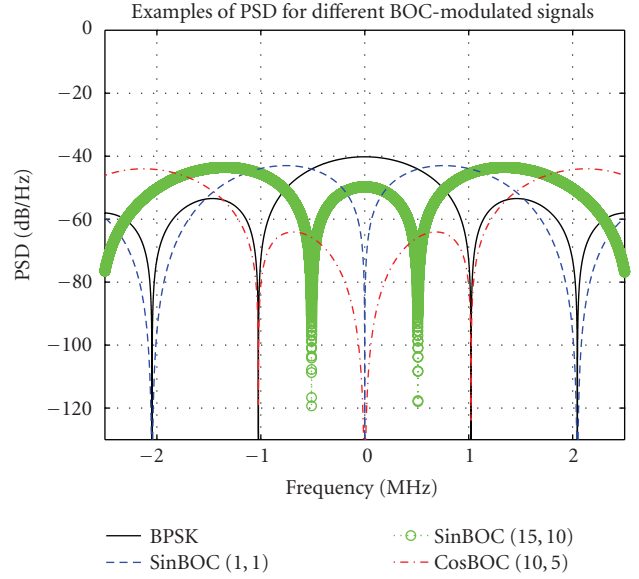

FIGURE 2: Examples of baseband PSD for BOC-modulated signals.

SinBOC(15, 10)), the interference around the DC frequency is not completely suppressed.

The baseband model of the received signal $r(t)$ via a fading channel can be written as [25]

$$r(t) = \sqrt{E_b}e^{+j2\pi f_D t} \sum_{n=-\infty}^{n=+\infty} b_n \sum_{l=1}^{L} \alpha_{n,l}(t) \\ \times s_{n,\sin/\mathrm{CosBOC}}(t - \tau_l) + \eta(t), \tag{6}$$

where E_b is the bit or symbol energy of signal (one symbol is equivalent with a code epoch and typically has a duration of $T = 1\,\mathrm{ms}$), f_D is the Doppler shift introduced by channel, L is the number of channel paths, $\alpha_{n,l}$ is the time-varying complex fading coefficient of the lth path during the nth code epoch, τ_l is the corresponding path delay (assuming to be constant or slowly varying during the observation interval) and $\eta(\cdot)$ is the additive noise component which incorporates the additive white noise from the channel and the interference due to other satellites.

At the receiver, the code-Doppler acquisition and tracking of the received signal (i.e., estimating the Doppler shift f_D and the channel delay τ_l) are based on the correlation with a reference signal $s_{\mathrm{ref}}(t - \hat{\tau}, \hat{f}_D, n_1)$, including the PRN code and the BOC modulation (here, n_1 is the considered symbol index):

$$s_{\mathrm{ref}}(t - \hat{\tau}, \hat{f}_D, n_1) \\ = e^{-j2\pi \hat{f}_D t} \sum_{k=-1}^{S_F} c_{k,n_1} \sum_{i=0}^{N_{\mathrm{BOC}_1}-1} \sum_{j=0}^{N_{\mathrm{BOC}_2}-1} (-1)^{i+j} p_{T_B} \\ \left(t - n_1 T - k T_c - i\frac{T_c}{N_{\mathrm{BOC}_1}} - j\frac{T_c}{N_{\mathrm{BOC}_1}N_{\mathrm{BOC}_2}} - \hat{\tau}\right). \tag{7}$$

Some examples of the absolute value of the ideal ACF for several BOC-modulated PRN sequences, together with the

BPSK case, are illustrated in Figure 3. As it can be observed, for any BOC-modulated signal, there are ambiguities within the ±1 chips interval around the maximum peak.

After correlation, the signal is coherently averaged over N_c ms, with the maximum coherence integration length dictated by the coherence time of the channel, by possible residual Doppler shift errors and by the stability of oscillators. If the coherent integration time is higher than the coherence time of the channel, the spectrum of the received signal will be severely distorted. The Doppler shift due to satellite movement is estimated and removed before performing the coherent integration. For further noise reduction, the signal can be noncoherently averaged over N_{nc} blocks; however there are some squaring losses in the signal power due to noncoherent averaging. The delay estimation is performed on a code-Doppler search space, whose values are averaged correlation functions with different time and frequency lags, with maxima occurring at $f = f_D$ and $\tau = \tau_l$.

3. EXISTING DELAY ESTIMATION ALGORITHMS IN MULTIPATH CHANNELS

The presence of multipath is an important source of error for GPS and Galileo applications. As mentioned before, traditionally, the multipath delay estimation block is implemented via a feedback loop. These tracking loop methods are based on the assumption that a coarse delay estimate is available at receiver, as result of the acquisition stage. The tracking loop is refining this estimate by keeping the track of the previous estimate.

3.1. Narrow early minus late (NEML) correlator

One of the first approaches to reduce the influences of code multipath is the narrow early minus late correlation method, first proposed in 1992 for GPS receivers [8]. Instead of using a standard correlator with an early late spacing Δ of 1 chip, a smaller spacing (typically $\Delta = 0.1$ chips) is used. Two correlations are performed between the incoming signal $r(t)$ and a late (resp., early) version of the reference code $s_{\mathrm{ref}_{\mathrm{Early,Late}}}(t - \hat{\tau} \pm \Delta/2)$, where $s_{\mathrm{ref}_{\mathrm{Early,Late}}}(\cdot)$ is the advanced or delayed BOC-modulated PRN code and $\hat{\tau}$ is the tentative delay estimate. The early (resp., late) branch correlations $R_{\mathrm{early,Late}}(\cdot)$ can be written as

$$R_{\mathrm{Early,Late}}(\hat{\tau}) = \int_{N_c} r(t) s_{\mathrm{ref}_{\mathrm{Early,Late}}}\left(t - \hat{\tau} \pm \frac{\Delta}{2}\right) dt. \qquad (8)$$

These two correlators spaced at Δ (e.g., $\Delta = 0.1$ chips) are used in the receiver in order to form the discriminator function. If channel and data estimates are available, the NEML loops are coherent. Typically, due to low CNR and residual Doppler errors from GPS and Galileo systems, noncoherent NEML loops are employed, when squaring or absolute value are used in order to compensate for data modulation and channel variations. The performance of NEML is best illustrated by the S-curve, which presents the expected value of error as a function of code phase error. For NEML, the two
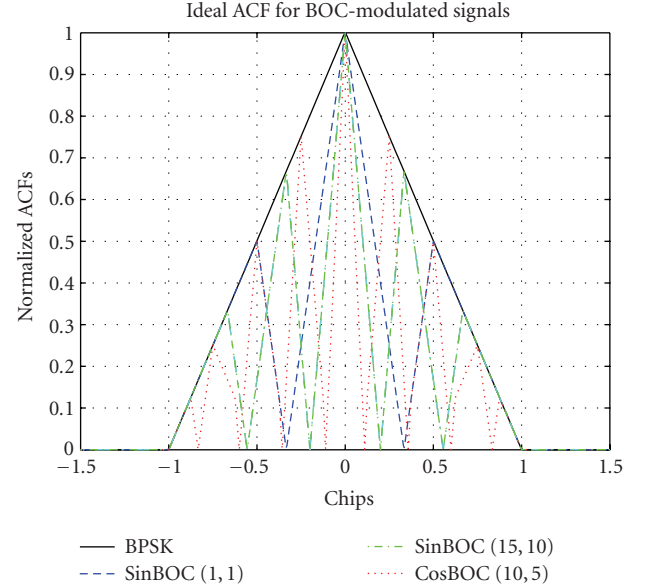

Figure 3: Examples of absolute value of the ACF for BOC-modulated signals.

branches are combined noncoherently, and the S-curve is obtained as in (9),

$$S_{\mathrm{NEML}}(\hat{\tau}) = \left| R_{\mathrm{Late}}(\hat{\tau}) \right|^2 - \left| R_{\mathrm{Early}}(\hat{\tau}) \right|^2. \qquad (9)$$

The error signal given by the S-curve is fed back into a loop filter and then into a numeric controlled oscillator (NCO) which advances or delays the timing of the reference signal generator. Figure 4 illustrates the S-curve in single path channel, for BPSK, SinBOC(1, 1), respectively, SinBOC(10, 5) modulated signals. The zerocrossing shows the presence of channel path, that is, the zero delay error corresponds to zero feedback error. However, for BOC-modulated signals, due to sidelobes ambiguities, the early late spacing should be less than the width of the main lobe of the ACF envelope, in order to avoid the false locks. Typically, for BOC(m, n) modulation, this translates to approximately $\Delta \le n/4m$.

3.2. High-resolution correlator (HRC)

The high-resolution correlator (HRC), introduced in [10], can be obtained using multiple correlator outputs from conventional receiver hardware. There are a variety of combinations of multiple correlators which can be used to implement the HRC concept, which yield similar performance. The HRC provides significant code multipath mitigation for medium and long delay multipath, compared to the conventional NEML detector, with minor or negligible degradation in noise performance. It also provides substantial carrier phase multipath mitigation, at the cost of significantly degraded noise performance, but, it does not provide rejection of short delay multipath [10]. The block diagram of a noncoherent HRC is shown in Figure 5. In contrast to the NEML structure, two new branches are introduced, namely, a very
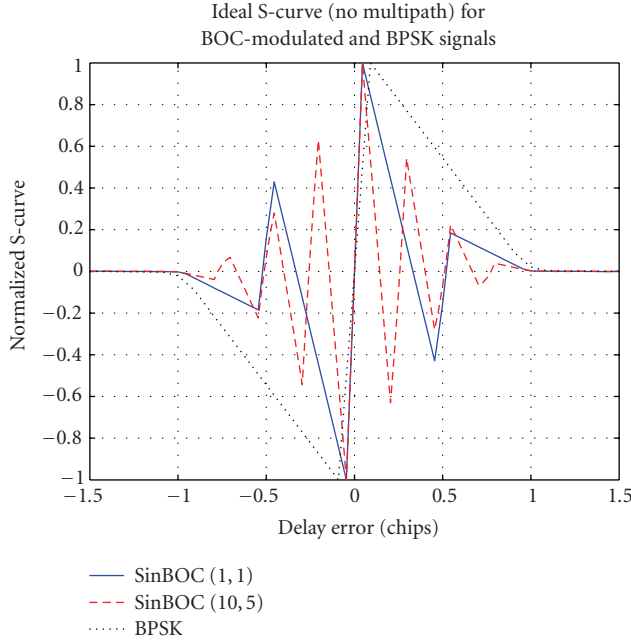
Figure 4: Ideal S-curves for BOC-modulated and BPSK signals (NEML, $\Delta = 0.1$ chips).

Figure 6: Ideal S-curves for noncoherent HRC with $a = -1/2$, for two BOC-modulated signals and $\Delta = 0.1$ chips.
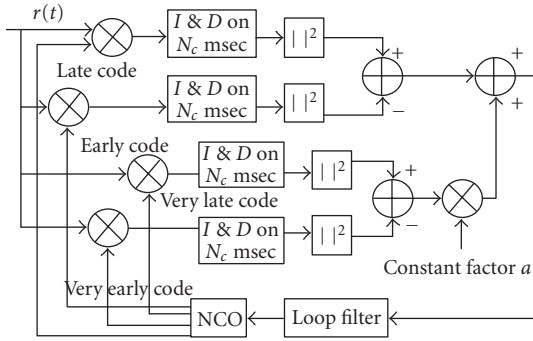

Figure 5: Block diagram for HRC tracking loop.

early and, respectively, a very late branch. The S-curve for a noncoherent five-correlator HRC can be written as in [10]:

$$
\begin{aligned}
S_{\text{HRC}}(\hat{\tau}) = {} & \left| R_{\text{Late}}(\hat{\tau}) \right|^2 - \left| R_{\text{Early}}(\hat{\tau}) \right|^2 \\
& + a \left(\left| R_{\text{VeryLate}}(\hat{\tau}) \right|^2 - \left| R_{\text{VeryEarly}}(\hat{\tau}) \right|^2 \right),
\end{aligned}
\tag{10}
$$

where $R_{\text{VeryLate}}(\cdot)$ and $R_{\text{VeryEarly}}(\cdot)$ are the very late and very early correlations, with the spacing between them of 2Δ chips, and a is a weighting factor which is typically $-1/2$ [10].

Examples of S-curves for HRC in the presence of a single path static channel, are shown in Figure 6, for two BOC-modulated signals. The early late spacing is $\Delta = 0.1$ chips (i.e., narrow correlator), thus the main lobes around zero crossing are narrower, and it is more likely that the separation between multiple paths will be done more easily.
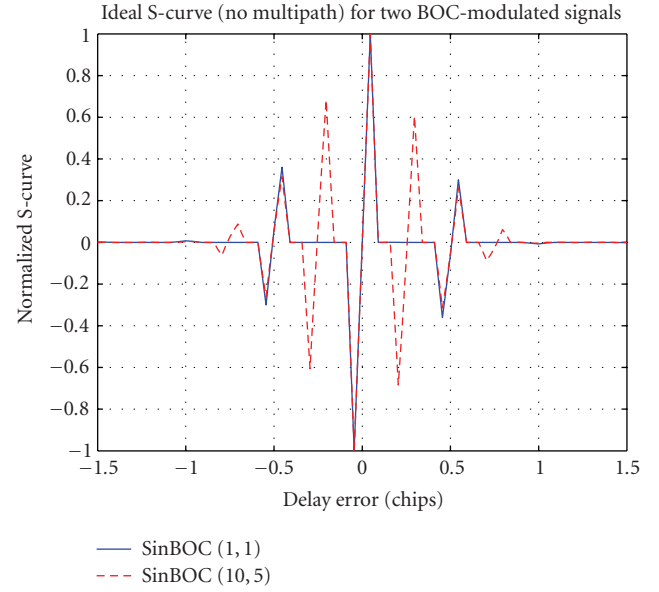
3.3. Multipath estimating delay locked loop (MEDLL)

A different approach, proposed to remove the multipath effects for GPS C/A delay tracking is the multipath estimation delay locked l;oop [15]. The MEDLL method estimates jointly the delays, phases, and amplitudes of all multipaths, canceling the multipath interference. Since it is not based on an S-curve, it can work in both feedback and feedforward configurations. To the authors' knowledge, the performance of MEDLL algorithm for BOC modulated signals is still not well understood, therefore, would be interesting to study a similar approach. The steps of the MEDLL algorithm (as implemented by us) are summarized bellow.

(i) Calculate the correlation function $R_n(t)$ for the nth transmitted code epoch. Find out the maximum peak of the correlation function and the corresponding delay $\hat{\tau}_1$, amplitude $\hat{a}_{1,n}$, and phase $\hat{\theta}_{1,n}$.

(ii) Subtract the contribution of the calculated peak, in order to have a new approximation of the correlation function $R_n^{(1)}(\tau) = R_n(\tau) - \hat{a}_{1,n} R_{\text{ref}}(t - \hat{\tau}_{1,n}) e^{j\hat{\theta}_{1,n}}$. Here $R_{\text{ref}}(\cdot)$ is the reference correlation function, in the absence of multipaths (which can be, for example, stored at the receiver). Find out the new peak of the residual function $R_n^{(1)}(\cdot)$ and its corresponding delay $\hat{\tau}_{2,n}$, amplitude $\hat{a}_{2,n}$, and phase $\hat{\theta}_{2,n}$. Subtract the contribution of the new peak of residual function from $R_n^{(1)}(t)$ and find a new estimate of the first peak. For more than two peaks, the procedure is continued until all desired peaks are estimated.

(iii) The previous step is repeated until a certain criterion of convergence is met, that is, when residual function is below a threshold (e.g., set to 0.5 here) or until
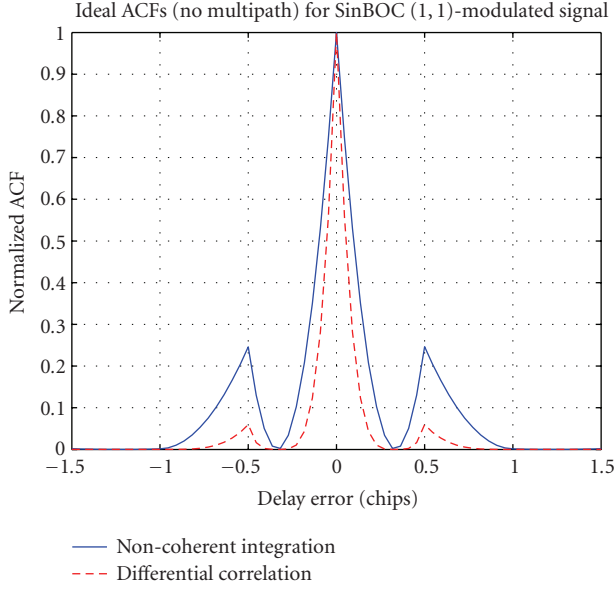
FIGURE 7: Envelope correlation function of traditional noncoherent integration and differential correlation for a SinBOC(1, 1)-modulated signal.

the moment when introducing a new delay does not improve the performance in the sense of root mean square error between the original correlation function and the estimated correlation function.

3.4. Differential correlation (DC)

Originally proposed for CDMA-based wireless communication systems, the differential correlation method has also been investigated in context of GPS navigation system [22]. It has been observed that with low and medium coherent times of the fading channel and in absence of any frequency error, this approach provides better resistance to noise than the traditional noncoherent integration methods. In DC method, the correlation is performed between two consecutive outputs of coherent integration. These correlation variables are then integrated, in order to obtain a differential variable. The differential detection variable z is given as

$$z_{DC} = \frac{1}{M-1} \sum_{k=1}^{M-1} |y_k^* y_{k+1}|^2, \tag{11}$$

where y_k, $k = 1, \ldots, M$ are the outputs of the coherent integration and M is the differential integration length. For a fair comparison between the differential noncoherent and traditional noncoherent methods, here it is assumed that $M = N_{nc}$, where N_{nc} is the noncoherent integration length. Since the differential coherent correlation method was noticed to be more sensitive to residual Doppler errors, only the differential noncoherent correlation is considered here.

The analysis done in [22] is limited to BPSK modulation. From Figure 7, it can be noticed that applying the DC to a BOC-modulated signal, instead of the conventional noncoherent integration, the sidelobes envelope can be decreased,

and thus this method has a potential in reducing the side peaks ambiguities.

3.5. Nonambiguous BOC(n, n) signal tracking (Julien&al. method)

A recent tracking approach, which removes the sidelobes ambiguities of SinBOC(n, n) signals and offers an improved resistance to long-delay multipath, has been introduced in [20]. This method, referred here as *Julien&al. method*, after the name of the first author in [20], has emerged while observing the ACF of a SinBOC(1, 1) signal with sine phasing, and the cross correlation of SinBOC(1, 1) signal with its spreading sequence. The ideal correlation function $R_{BOC}^{ideal}(\cdot)$ for SinBOC(1, 1)-modulated signals in the absence of multipaths, can be written as [25]

$$R_{BOC}^{ideal}(\tau) = \Lambda_{T_c/2}(\tau) - \frac{1}{2}\Lambda_{T_c/2}\left(\tau - \frac{T_c}{2}\right) - \frac{1}{2}\Lambda_{T_c/2}\left(\tau + \frac{T_c}{2}\right), \tag{12}$$

where $\Lambda_{T_c/2}(\tau - \alpha)$ is the value in τ of a triangular function[1] centered in α, with a width of 1-chip, T_c is the chip period, and τ is the code delay in chips.

The cross correlation of a SinBOC(1, 1) signal with the spreading pseudorandom code, for an ideal case (no multipaths and ideal PRN code), can be expressed as [20]

$$R_{BOC,PRN}^{ideal}(\tau) = \frac{1}{2}\left(\Lambda_{T_c/2}\left(\tau + \frac{T_c}{2}\right) + \Lambda_{T_c/2}\left(\tau - \frac{T_c}{2}\right)\right). \tag{13}$$

Two types of DLL discriminators have been considered in [20], namely, the early-minus- late- power (EMLP) discriminator and the dot-product (DP) discriminator. These examples of possible discriminators result from the use of the combination of BOC-autocorrelation function and of the BOC/PRN-correlation function [20]. Based on (12) and (13), the ideal EMLP discriminator is constructed, as in (14), where τ is the code tracking error [20]:

$$S_{EMLP}^{ideal}(\tau) = \left[R_{BOC}^{ideal^2}\left(\tau + \frac{\Delta}{2}\right) - R_{BOC}^{ideal^2}\left(\tau - \frac{\Delta}{2}\right)\right] - \left[R_{BOC,PRN}^{ideal^2}\left(\tau + \frac{\Delta}{2}\right) - R_{BOC,PRN}^{ideal^2}\left(\tau - \frac{\Delta}{2}\right)\right]. \tag{14}$$

The alternative DP discriminator variant [20] does not have a linear variation as a function of code tracking error:

$$S_{DP}^{ideal}(\tau)$$
$$= \left[R_{BOC}^{ideal^2}\left(\tau + \frac{\Delta}{2}\right) - R_{BOC}^{ideal^2}\left(\tau - \frac{\Delta}{2}\right)\right]R_{BOC}^{ideal^2}(\tau)$$
$$- \left[R_{BOC,PRN}^{ideal^2}\left(\tau + \frac{\Delta}{2}\right) - R_{BOC,PRN}^{ideal^2}\left(\tau - \frac{\Delta}{2}\right)\right]R_{BOC}^{ideal^2}(\tau). \tag{15}$$

---

[1] Our notation is equivalent with the notation $tri_\alpha(x/y)$ used in [20], via $tri_\alpha(\tau/y) = \Lambda_{T_c/2}(\tau - \alpha T_c/y)$.

SinBOC (1, 1) modulation, ACFs of
BOC-modulated and subtracted signals

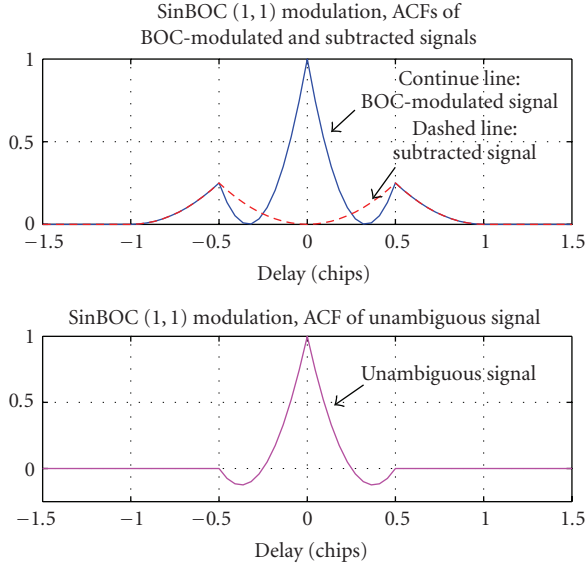SinBOC (1, 1) modulation, ACF of unambiguous signal

FIGURE 8: SinBOC(1, 1)-modulated signal: examples of the ambiguous correlation function and subtracted pulse (upper plot) and the obtained unambiguous correlation function (lower plot), for a single-path channel.

Since the resulting discriminators remove the effect of SinBOC(1, 1) modulation, there are no longer false lock points, and the narrow structure of the main correlation lobe is preserved [20]. Indeed, the side peaks of SinBOC(1, 1) correlation function $R_{\text{BOC}}^{\text{ideal}}(\tau)$ have the same magnitude and same location as the two peaks of SinBOC(1, 1)/PRN-correlation function $R_{\text{BOC,PRN}}^{\text{ideal}}(\tau)$. By subtracting the squares of the two functions, a new synthesized correlation function is derived and the two side peaks of SinBOC(1, 1) correlation function are canceled almost totally, while still keeping the sharpness of the main lobe (Figure 8). Two small negative sidelobes appear next to the main peak (about ± 0.35 chips around the global maximum), but since they point downwards, they do not bring any threat [20]. The correlation values spaced at more than 0.5 chips apart from the global peak are very close to zero, which means a potentially strong resistance to long-delay multipath.

In practice, the discriminators $S_{\text{EMLP}}(\tau)$ or $S_{\text{DP}}(\tau)$, as given in [20], are formed via continuous computation, at receiver side, of correlation functions $R_{\text{BOC}}(\cdot)$ and $R_{\text{BOC,PRN}}(\cdot)$ values, not on the ideal ones. In practice, $R_{\text{BOC}}(\cdot)$ is the correlation between the incoming signal (in the presence of multipaths) and the reference BOC-modulated code, and $R_{\text{BOC,PRN}}(\cdot)$ is the correlation between the incoming signal and the pseudorandom code (without BOC modulation). This method has been applied only to SinBOC(n, n) signals. Moreover, instead of making use of the ideal reference function $R_{\text{BOC,PRN}}^{\text{ideal}}(\cdot)$ (which can be computed only once and stored at the receiver side), the correlation $R_{\text{BOC,PRN}}(\cdot)$ needs to be computed for each code epoch in [20]. Of course, in order to make use of the $R_{\text{BOC,PRN}}^{\text{ideal}}(\cdot)$ shape, we also need some information about channel multipath profile. This will be explained in the next section.

4. SIDELOBES CANCELLATION METHOD (SCM)

In this section, we introduce unambiguous tracking approaches based on sidelobe cancellation; all these approaches are grouped under the generic name of *sidelobes cancellation methods*). The SCM technique removes or diminishes the threats brought by the sidelobes peaks of the BOC-modulated signals. In contrast with the Julien&al. method, which is restricted to the SinBOC(n, n) case, we will show here how to use SCM with any sine or cosine BOC-modulated signal. The SCM approach uses an ideal reference correlation function at receiver, which resembles the shapes of sidelobes, induced by BOC modulation. In order to remove the sidelobes ambiguities, this ideal reference function is subtracted from the correlation of the received BOC-modulated signal with the reference PRN code. In the Julien&al. method, the subtraction function, which approximates the sidelobes, is provided by cross-correlating the spreading PRN code and the received signal. Here, this subtraction function is derived theoretically, and computed only once per BOC signal. Then, it is stored at the receiver side in order to reduce the number of correlation operations. Therefore, our methods provide a less time-consuming and simpler approach, since the reference ideal correlation function is generated only once and can be stored at receiver.

4.1. Ideal reference functions for SCM method

In this subsection, we explain how the subtraction pulses are computed and then applied to cancel the undesired sidelobes.

Following derivations similar with those from [25] and intuitive deductions, we have derived the following ideal reference function to be subtracted from the received signal after the code correlation:

$$R_{\text{sub}}^{\text{ideal}}(\tau) = \sum_{i=0}^{N_{\text{BOC}_1}-1} \sum_{j=0}^{N_{\text{BOC}_1}-1} \sum_{k=0}^{N_{\text{BOC}_2}-1} \sum_{l=0}^{N_{\text{BOC}_2}-1}$$
$$(-1)^{i \times j + k + l} \Lambda_{T_B}\left(\tau + (i - j)T_B + (k - l)\frac{T_B}{N_{\text{BOC}_2}}\right),$$
$$(16)$$

where $T_B = T_c/N_{\text{BOC}_1}N_{\text{BOC}_2}$ is the BOC interval, $\Lambda_{T_B}(\cdot)$ is the triangular function centered at 0 and with a width of $2T_B$-chips, N_{BOC_1} is the sine BOC-modulation order (e.g., $N_{\text{BOC}_1} = 2$ for SinBOC(1, 1), or $N_{\text{BOC}_1} = 4$ for SinBOC(10, 5)) [25], and N_{BOC_2} is the second BOC-modulation factor which covers sine and cosine cases, as explained in [25] (i.e., if sine BOC modulation is employed, $N_{\text{BOC}_2} = 1$ and, if cosine BOC modulation is employed, $N_{\text{BOC}_2} = 2$).

As an example, the simplest case of SinBOC(1, 1)-modulation (i.e., the main choice for Open Services in Galileo), (16) becomes

$$R_{\text{sub,SinBOC(1,1)}}^{\text{ideal}}(\tau) = \left(\Lambda_{T_B}(\tau - T_B) + \Lambda_{T_B}(\tau + T_B)\right), \quad (17)$$

which is similar with Julien& al. expression of (13) with the exception of a 1/2 factor (here, $T_B = T_c/2$).

The Sin- and CosBOC(m, n)-based ideal autocorrelation function can be written as [25]

$$R_{\text{BOC}}^{\text{ideal}}(\tau) = \sum_{i=0}^{N_{\text{BOC}_1}-1} \sum_{j=0}^{N_{\text{BOC}_1}-1} \sum_{k=0}^{N_{\text{BOC}_2}-1} \sum_{l=0}^{N_{\text{BOC}_2}-1}$$
$$(-1)^{i+j+k+l} \Lambda_{T_B}\left(\tau + (i-j)T_B + (k-l)\frac{T_B}{N_{\text{BOC}_2}}\right). \tag{18}$$

Again, for SinBOC(1, 1) case, the expression of (18) reduces to

$$R_{\text{SinBOC}(1,1)}^{\text{ideal}}(\tau)$$
$$= (2\Lambda_{T_B}(\tau) - \Lambda_{T_B}(\tau - T_{\text{BOC}}) - \Lambda_{T_B}(\tau + T_{\text{BOC}})), \tag{19}$$

which is, again, similar to Julien& al. expression of (12) with the exception of a 1/2 factor (for SinBOC(1, 1), $T_{\text{BOC}} = T_c/2$, $N_{\text{BOC}_1} = 2$ and $N_{\text{BOC}_2} = 1$).

We remark that the difference between (16) and (18) stays in the power of -1 factor, that is, (16) stands for an approximation of the sidelobe effects (no main lobe included), while (18) is the overall ACF (including both the main lobe and the side lobes). The next step consists in canceling the effect of sidelobes (16) from the overall correlation (18), after normalizing them properly.

Thus, in order to obtain an unambiguous ACF shape, the squared function $(R_{\text{sin}}^{\text{ideal}}(\cdot))^2$, $(R_{\text{cos}}^{\text{ideal}}(\cdot))^2$, respectively, has to be subtracted from the ambiguous squared correlation function as shown in

$$R_{\text{unamb}}^{\text{ideal}}(\tau) = \left(R_{\text{BOC}}^{\text{ideal}}(\tau)\right)^2 - w\left(R_{\text{sin/cos}}^{\text{ideal}}(\tau)\right)^2, \tag{20}$$

where $w < 1$ is a weight factor used to normalize the reference function (to achieve a magnitude of 1).

For example, for SinBOC(1, 1) and $w = 1$, we get from (17), (19), and (20), after straightforward computations, that

$$R_{\text{unamb}}^{\text{ideal}}(\tau) = 4\big(\Lambda_{T_B}^2(\tau) - \Lambda_{T_B}(\tau)\Lambda_{T_B}(\tau - T_{\text{BOC}}) \\ - \Lambda_{T_B}(\tau)\Lambda_{T_B}(\tau + T_{\text{BOC}})\big), \tag{21}$$

and if we plot $R_{\text{unamb}}^{\text{ideal}}(\tau)$ (e.g., see the lower plot of Figure 8), we get a main narrow correlation peak, without sidelobes.

All the derivations so far were based on ideal assumptions (ideal correlation codes, single path static channels, etc.). However, in practice, we have to cope with the real signals, so the ideal autocorrelation function $R_{\text{BOC}}^{\text{ideal}}(\tau)$ should be replaced with the computed correlation $R_{\text{BOC}}(\tau)$ between the received signal and the reference BOC-modulated pseudo-random code. Thus, (20) becomes

$$R_{\text{unamb}}(\tau) = \left(R_{\text{BOC}}(\tau)\right)^2 - w\left(R_{\text{sin/cos}}^{\text{ideal}}(\tau)\right)^2. \tag{22}$$

Here comes into equation the weighting factor, since various channel effects (such as noise and multipath) can modify the levels of $R_{\text{BOC}}(\tau)$ function. In order to perform the
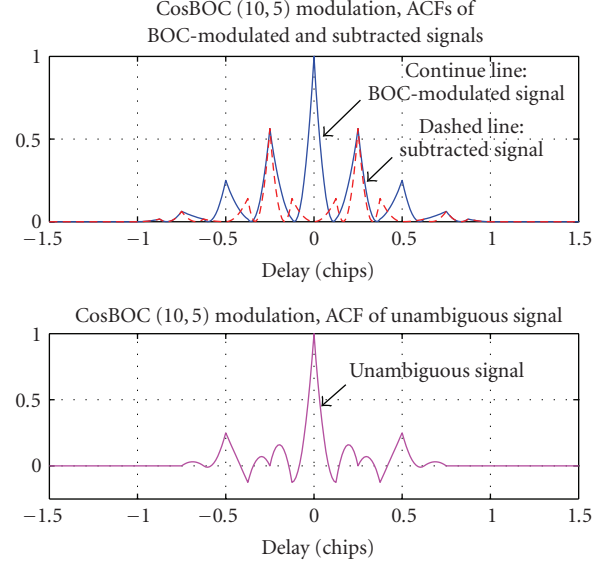

FIGURE 9: CosBOC(10, 5)-modulated signal: examples of the ambiguous correlation function and subtracted pulse (upper plot) and obtained unambiguous correlation function (lower plot), in a single-path channel.

normalization of reference function (i.e., to find the weight factors w), the peaks magnitudes of $R_{\text{BOC}}(\cdot)$ function are first found out and sorted in increased order. Then the weighting factor w is computed as the ratio between the last-but-one peak and the highest peak. We remark that the above algorithm does not require the computation of the BOC/PRN correlation anymore, it only requires the computation of $R_{\text{BOC}}(\tau) = R_n(\tau)$ correlation. The pulses to be subtracted are always based on the ideal functions $R_{\text{sin/cos}}^{\text{ideal}}(\tau)$, and therefore, they can be computed only once (via (16)) and stored at the receiver (in order to decrease the complexity of the tracking unit).

By comparison with Julien&al. method, here the number of correlations at the receiver is reduced by half (i.e., $R_{\text{BOC,PRN}}(\cdot)$ computation is not needed anymore). Thus the SCM technique offers less computational burden (only one correlation channel in contrast to Julien&al. method, which uses two correlation channels).

Figures 8 and 9 show the shapes of the ideal ambiguous correlation functions and of the subtracted pulses, together with the correlation functions, obtained after subtraction (SCM method). Figure 8 exemplifies a SinBOC(1, 1)-modulated signal, while Figure 9 illustrates the shapes for a CosBOC(10, 5)-modulation case. As it can be observed, for both SinBOC and CosBOC modulations, the subtractions removes the sidelobes closest to the main peak, which are the main threats in the tracking process. Also, it should be mentioned that the Figure 8, for a SinBOC(1, 1) modulated signal, is also illustrative for the Julien&al. method, since the shapes of correlation functions are similar with those presented in [20].

Equation (20) is valid for single path channels. However, in multipath presence, delay errors due to multipaths

are likely to appear. When (22) is applied in this situation, one important issue is to align the subtraction pulse to the LOS peak (otherwise, the subtraction of (22) will not cancel the correct sidelobes). This can be done only if some initial estimate of LOS delay is obtained. For this purpose, we employ and compare several feedback loops or feedforward algorithms, as it will be explained next.

4.2. SCM with interference cancellation (IC)

Combining the multipath eliminating DLL concept with the SCM method, we obtain an improved SCM technique with multipath interference cancellation (*SCM with IC*). In this method, the initial estimate of LOS delay is obtained via MEDLL algorithm. The sidelobe cancellation is applied inside the iterative steps of MEDLL, as explained below.

(1) Calculate the correlation function $R_n(\tau)$ between the received signal and the reference BOC-modulated code (e.g., see the continuous line, Figure 10, upper plot). Find the global maximum peak (the peak 1) of this correlation function, $\max_\tau |R_n(\tau)|$, and its corresponding delay, $\hat{\tau}_{1,n}$, amplitude $\hat{a}_{1,n}$ and phase $\hat{\theta}_{1,n}$ (e.g., the peak situated at the 50th-sample delay, Figure 10, upper plot).

(2) Compute the ideal reference function centered at $\hat{\tau}_{1,n}$: $R_{sub}^{ideal}(\tau - \hat{\tau}_{1,n})$ via (16) (see the dashed line, Figure 10, upper plot).

(3) Build an initial estimate of the channel impulse response (CIR) based on $\hat{\tau}_{1,n}$, $\hat{a}_{1,n}$, and $\hat{\theta}_{1,n}$ (e.g., the estimated CIR of peak 1, Figure 10, upper plot).

(4) In order to remove the sidelobes ambiguities, the function $R_{sub}^{ideal}(\tau - \hat{\tau}_{1,n})$ is then subtracted from the multipath correlation function $R_n(\tau)$ and an unambiguous shape is obtained, using (22), or, equivalently $R_{n,unamb}(\tau) = (R_n(\tau))^2 - (R_{sub}^{ideal}(\tau - \hat{\tau}_{1,n}))^2$. In Figure 10, the unambiguous ACF $R_{n,unamb}(\cdot)$ is plotted with dashed-dotted line, in both upper and lower plots.

(5) Cancel out the contribution of the strongest path and obtain the residual function $R_{n,unamb}^{(1)}(\tau) = R_{n,unamb}(\tau) - \hat{a}_{1,n}R_{unamb}^{ideal}(\tau)(\tau - \hat{\tau}_{1,n})e^{j\hat{\theta}_{1,n}}$, where $R_{unmab}^{ideal}(\tau)$ is the unambiguous reference function given by (20). The shape of residual function is exemplified in Figure 10, lower plot (drawn with continuous line).

(6) The new maximum peak of the residual function $R_{n,unamb}^{(1)}$ is found out (e.g., at 44th-sample delay, Figure 10, lower plot), with its corresponding delay $\hat{\tau}_{2,n}$, amplitude $\hat{a}_{2,n}$ and phase $\hat{\theta}_{2,n}$. The contributions of both peaks 1 and 2 are subtracted from unambiguous correlation function $R_{n,unamb}(\tau)$

Exemplification of SCM IC method (steps 1 to 4)

Original ACF —— Subtracted ideal function ---
Estimated CIR —⊙— Unambiguous ACF —·—

Exemplification of SCM IC method (steps 5 to 6)

Unambiguous ACF —·—
Residual function ——
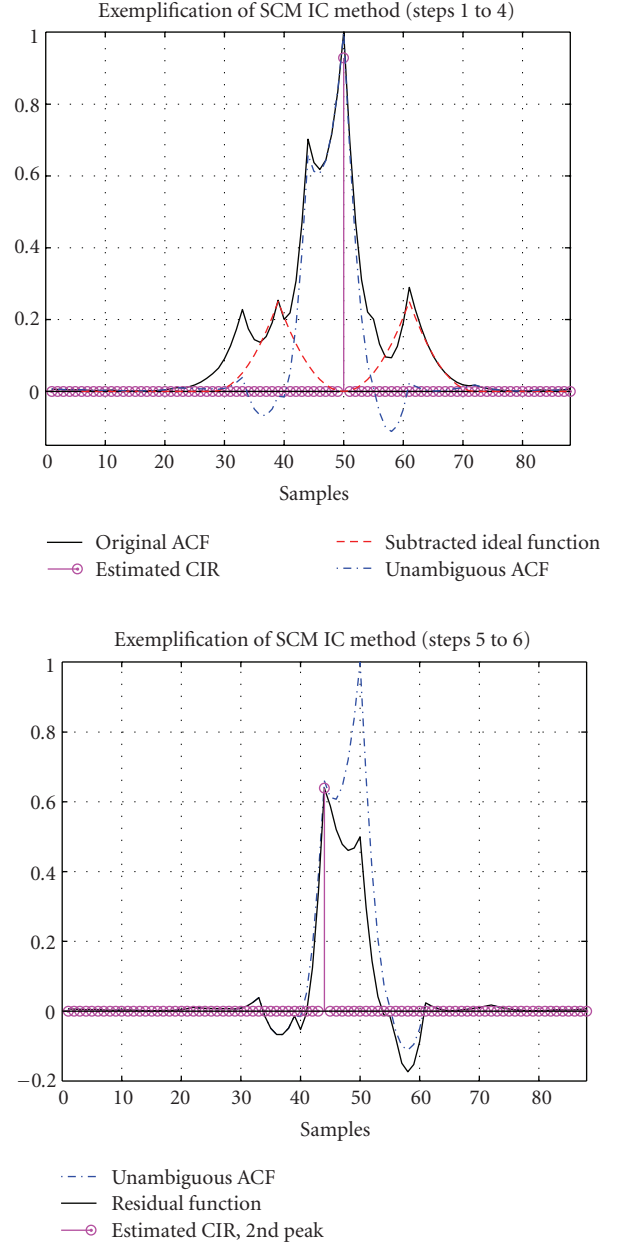Estimated CIR, 2nd peak —⊙—

FIGURE 10: Exemplification of SCM IC method, 2-paths fading channel with true channel delay at 44 and 50 samples, average path powers $[-2, 0]$ dB, SinBOC(1, 1)-modulated signal.

and the maximum global peak is re-estimated from
$$R_{n,unamb}^{(2)}(\tau) = (R_{n,unamb}(\tau))^2 - (\hat{a}_{1,n}R_{unamb}^{ideal}(\tau)(\tau - \hat{\tau}_{1,n})e^{j\hat{\theta}_{1,n}} + \hat{a}_{2,n}R_{unamb}^{ideal}(\tau)(\tau - \hat{\tau}_{2,n})e^{j\hat{\theta}_{2,n}})^2.$$

(7) The steps (3) to (6) are repeated until all desired peaks are estimated and until the residual function is below a threshold value. In the example of Figure 10, after 6 steps both path delays are estimated correctly.

These steps of SCM IC method are illustrated in Figure 10, for 2-path fading channel.
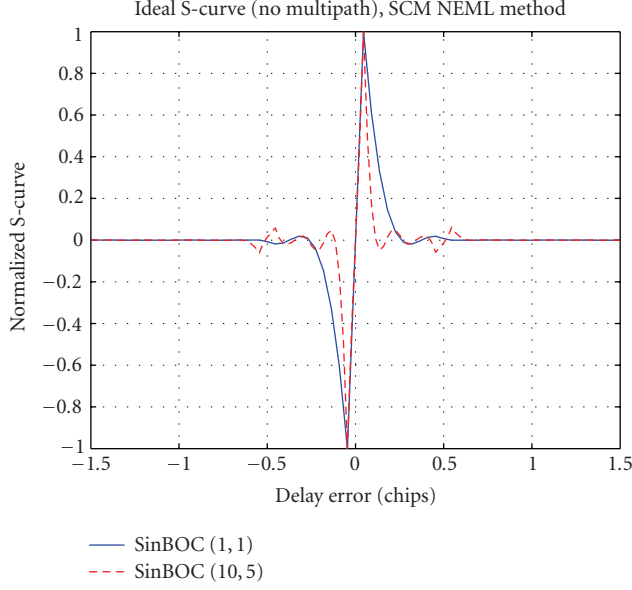
Figure 11: SCM NEML method: ideal S-curves (no multipath), for two BOC-modulation cases and $\Delta = 0.1$ chips.

Figure 12: Multipath error envelopes (in meters): NEML correlator versus SCM NEML method, for two BOC-modulation cases and $\Delta = 0.1$ chips.

4.3. SCM using narrow early minus lat discriminator (SCM NEML)

After obtaining an unambiguous correlation function $R_{n,\text{unamb}}(\tau)$ (as it was shown in the previous section, steps (1) to (4)), a NEML S-curve is constructed, by forming the early, respectively, late branches, spaced at $\Delta = 0.1$ chips. The S-curve is obtained in the same way as in Section 3.1, by subtracting the late and early branches of unambiguous correlation function,

$$S_{\text{SCM}_{\text{NEML}}}(\hat{\tau}) = \left| R_{n,\text{unamb}}^{\text{Late}}(\hat{\tau}) \right|^2 - \left| R_{n,\text{unamb}}^{\text{Early}}(\hat{\tau}) \right|^2. \quad (23)$$

Examples of S-curves obtained with this method, in presence of a single path static channel, are presented in Figure 11, for two BOC-modulated signals, SinBOC(1, 1) and SinBOC(10, 5), and a spacing of $\Delta = 0.1$ chips. Comparing with Figure 4, which presents the NEML S-curves for ambiguous signals, in Figure 11, the possibility to detect an incorrect zero crossing, due to sidelobes peaks, is decreased.

A typical measure of performance for the ability of a delay tracking loop to deal with multipath error is the so-called multipath error envelope (MEE) [9, 10]. The MEE is usually computed for one direct and one reflected channel paths, with a certain variable spacing. The multipath errors are calculated for the worst-case scenario, when the two paths are added inphase (upper MEE) and have equal strength, and also, when the two paths are out of phase (lower MEE). Comparisons of MEEs plots, for both NEML and SCM NEML methods, are shown in Figure 12, for two BOC-modulated signals. A static channel with two paths of equal amplitudes and variable spacing was considered. The only interference considered here is the multipath interference, and the additive white noise effect is not taken into account. As it can be seen in Figure 12, comparing with the NEML correlator, the
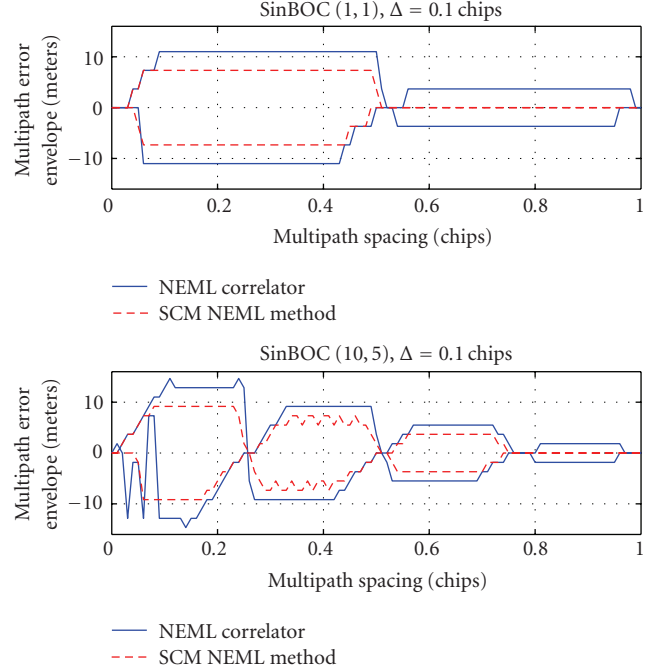
SCM NEML method brings a decrease in the errors of multipath envelopes, for both SinBOC(1, 1) and SinBOC(10, 5) signals. We remark that the variations of the lower delay error envelope in the lower plot of Figure 12 are due to, on one hand, the errors in the zero-crossing estimation algorithm, and, on the other hand, to the fact that worse MEE is not necessarily guaranteed when the paths are out of phase for the noncoherent NEML.

4.4. SCM using high-resolution correlator discriminator (SCM HRC)

In a similar manner as in previous section, the SCM method can be also used in conjunction with an HRC discriminator, after removing the side peaks threats and obtaining an unambiguous correlation function $R_{n,\text{unamb}}(\tau)$. Based on this unambiguous function, an HRC S-curve is constructed, in an analogous way as in Section 3.2:

$$\begin{aligned} S_{\text{SCM}_{\text{HRC}}}(\hat{\tau}) = {} & \left| R_{n,\text{unamb}}^{\text{Late}}(\hat{\tau}) \right|^2 - \left| R_{n,\text{unamb}}^{\text{Early}}(\hat{\tau}) \right|^2 \\ & + a \left(\left| R_{n,\text{unamb}}^{\text{VeryLate}}(\hat{\tau}) \right|^2 - \left| R_{n,\text{unamb}}^{\text{VeryEarly}}(\hat{\tau}) \right|^2 \right), \end{aligned}$$
$$(24)$$

where $R_{n,\text{unamb}}^{\text{Early}}(\cdot)$ and $R_{n,\text{unamb}}^{\text{Late}}(\cdot)$ are the advanced and delayed unambiguous correlations, with a spacing between them of $\Delta = 0.1$ chips. The $R_{n,\text{unamb}}^{\text{VeryEarly}}(\cdot)$, respectively, $R_{n,\text{unamb}}^{\text{VeryLate}}(\cdot)$ are the very early and the very late unambiguous correlation branches, spaced at 2Δ chips and the weighting factor $a = -1/2$.
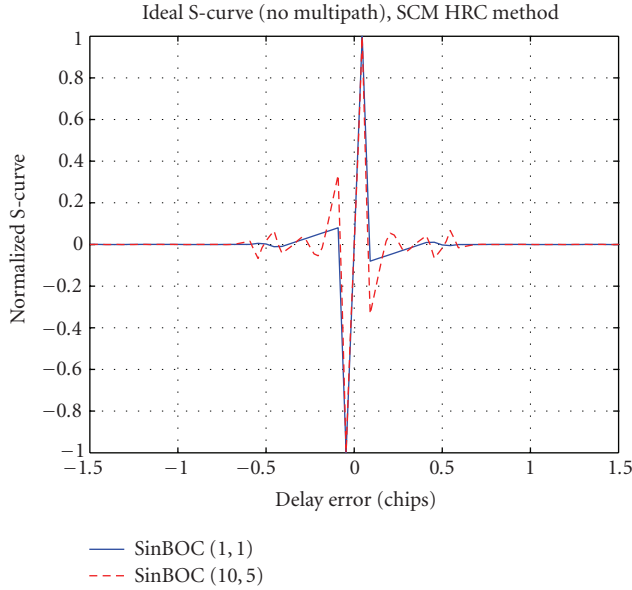
FIGURE 13: SCM HRC method: ideal S-curves (no multipath), for two BOCmodulation cases, with $a = -1/2$ and $\Delta = 0.1$ chips.
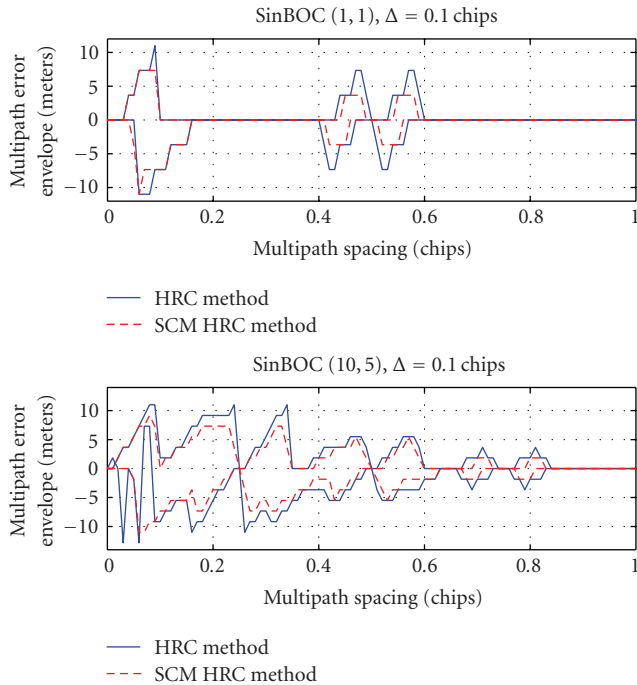

FIGURE 14: Multipath error envelopes (in meters): HRC method versus SCM HRC method, for two BOC-modulation cases and $\Delta = 0.1$ chips.

The ideal S-curves obtained with the SCM HRC method, for two BOC-modulation orders, are presented in Figure 13. The MEEs performances, for both the HRC and SCM HRC methods, are illustrated in Figure 14, for SinBOC(1, 1) and
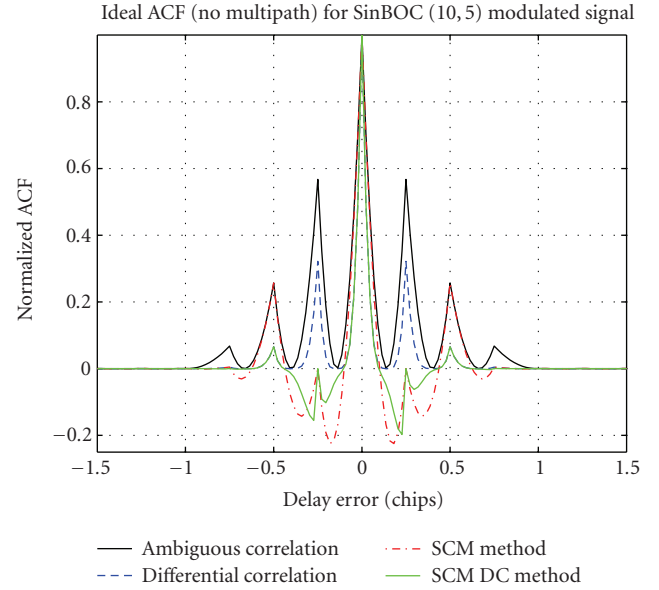

FIGURE 15: Envelopes of correlation functions obtained with ambiguous correlation, DC method, SCM approach, and SCM DC method, for a SinBOC(10, 5)-modulated signal.

SinBOC(10, 5) cases. As it can be noticed, there is a slight improvement brought by the SCM HRC method over the HRC correlator.

4.5. SCM using differential correlation (DC) in conjunction with feedback and feedforward tracking algorithms

It has been observed that the DC method has potential to decrease the sidelobes amplitudes, thus lowering the possibility to detect a wrong side peak. To enhance the performance of the DC method, we use it in conjunction with different tracking algorithms, such as NEML or HRC methods, or with IC method. These algorithms are applied in similar ways as explained in Sections 3.1, 3.2, and 3.3, on the correlation functions obtained after performing the noncoherent DC technique (Section 3.4).

Also, the performance may be enhanced further, by using the SCM approach after applying the DC method. This is done in the same way as explained in previous Sections (4.2, 4.3, and 4.4), but after using first the DC method on the ambiguous correlation function between the multipath received signal and the reference BOC-modulated code. Indeed, as illustrated in Figure 15, in case of a SinBOC(10, 5) modulated signal, the combination of DC and SCM algorithms can decrease even further the sidelobes amplitudes, thus eliminating more ambiguities.

4.6. SCM with threshold comparison (SCM thr)

Another approach is to test the performance of *SCM* technique using a *thresholding algorithm*. Starting from the unambiguous correlation function $R_{n,\text{unamb}}(\tau)$, an estimate of noise variance $\hat{\sigma}_n^2$ is obtained, as the mean of the squares of

the out-of-peak values, similar to [4]. Using this estimated noise variance, a linear threshold γ is computed, based on the second peak γ_2 of the ideal unambiguous correlation function $R_{\text{unamb}}^{\text{ideal}}(\tau)$ (i.e., for SinBOC(1, 1) $\gamma_2 = 0.5$, as seen in Figure 3), together with the estimate of the noise variance $\hat{\sigma}_n^2$:

$$\gamma = \gamma_2 + \sqrt{\hat{\sigma}_n^2}. \tag{25}$$

Then the LOS delay is estimated, based on the unambiguous correlation function $R_{n,\text{unamb}}(\tau)$, using this threshold. If the peak of the estimated first path is too low (i.e., ten times lower than the global peak), then this path is discarded and the next estimate is considered.

5. SIMULATION RESULTS

5.1. Additive white noise Gaussian (AWGN) channel

We first test the performance of the proposed algorithms in the ideal AWGN channel (single path), in order to check whether SCM algorithm introduces a deterioration with respect to the standard narrow and high-resolution correlators (it is known that NEML is able to attain the Cramer-Rao bound in AWGN channels [8]). We will show that no deterioration is incurred when SCM is applied. The performance criteria are root mean square error (RMSE) and mean time to lose lock (MTLL). The simulations were carried out in Matlab. The MTLL is computed as the average value for which the estimated delay tracking error of the first path is below 1 chip. The tracking process is started, after the coarse acquisition of the signal, assuming that we are in the "lock" condition, that is, the delay error is strictly less than one chip. For all presented simulations (both in this section and in Section 5.2), the coherent integration length is set to $N_c = 20$ milliseconds and the noncoherent integration is performed over $N_{\text{nc}} = 3$ blocks (i.e., the total coherent and non-coherent integration length is 60 milliseconds), and the oversampling factor is set to $N_s = 11$. We generated 5000 random points in order to compute the RMSE and MTLL statistics. That is, the maximum observable MTLL based on these simulations is $5000 N_c N_{\text{nc}} = 300$ s (i.e., an MTTL value of 300 seconds reflects the fact that we never lost the lock during that particular simulation).

The AWGN results are shown for SinBOC(1, 1) case in Figures 16 and 17, for the comparison with NEML and HRC, respectively. As seen in these figures, SCM algorithm does not deteriorate the performance in AWGN case, compared with narrow and high-resolution correlators. The sidelobe cancellations applied on the top of NEML and HRC give the same results as those of the original NEML and HRC algorithms, respectively, if the channel is single path AWGN channel (e.g., the differences in performance between SCM + NEML and NEML are only at the third decimal, with NEML slightly better).

5.2. Fading channels

In what follows, the performance of the discussed delay estimation algorithms is compared in multipath fading chan-
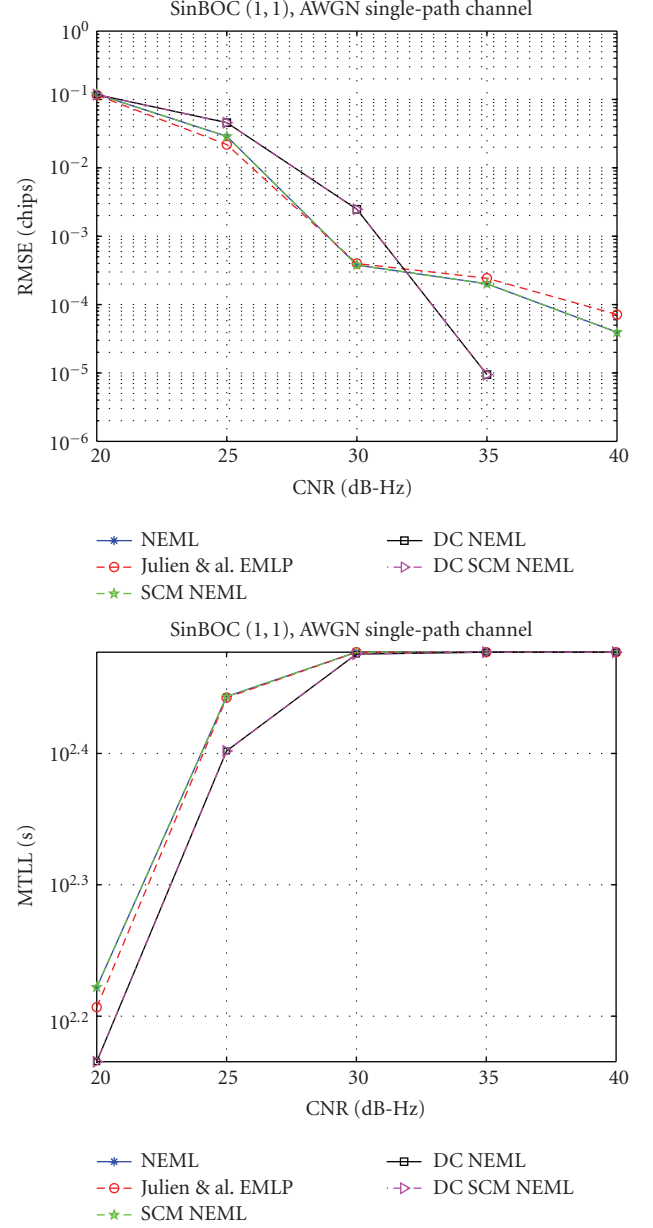

FIGURE 16: Comparison of feedback delays estimation algorithms employing the NEML discriminator and of the Julien&al. method, as a function of CNR; upper plots: RMSE, lower plots: MTLL. NEML and SCM NEML curves are overlapping. DC NEML and DC SCM NEML curves are also overlapping (differences at the 3rd decimal).

nels. The same performance criteria as in the previous section are used, namely, RMSE and MTLL. Two representative BOC-modulated signals have been selected for the simulations included in this paper. The first one is the SinBOC(1, 1) modulation, the common baseline for Galileo open service (OS) structure, agreed by US and European negotiation. The second one is the CosBOC(10, 5) modulation, which has been proposed for the Galileo Public Regulated Service (PRS) and for the current GPS M-code. In order to have fair

SinBOC $(1, 1)$, AWGN single-path channel

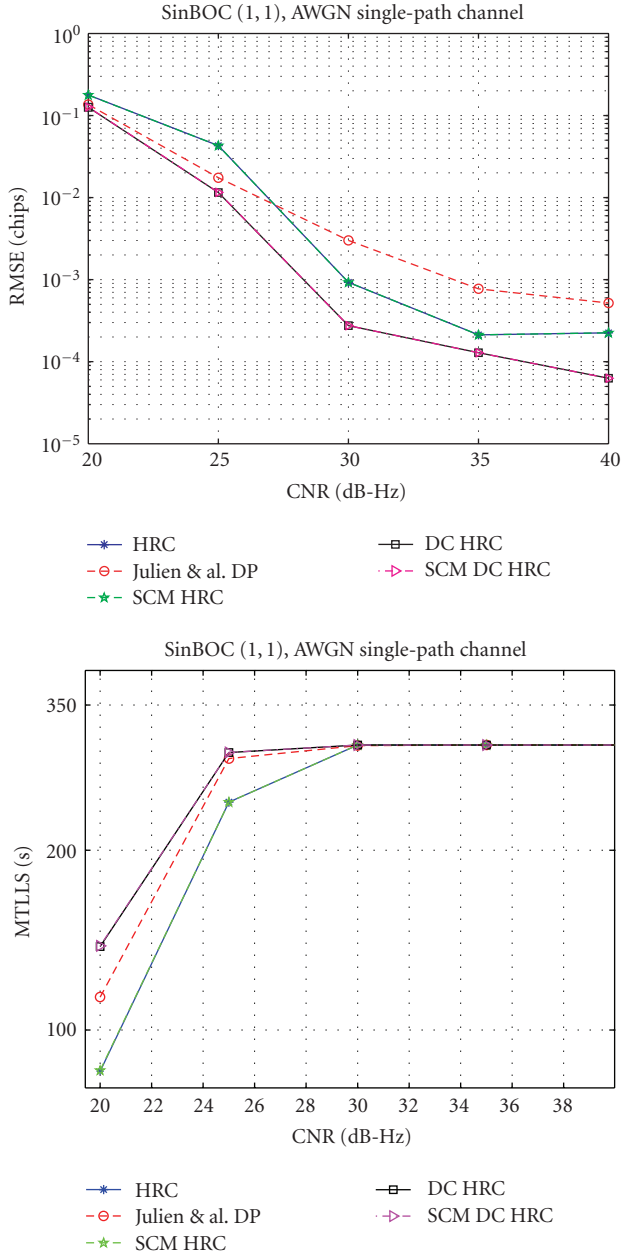SinBOC $(1, 1)$, AWGN single-path channel

FIGURE 17: Comparison of feedback delays estimation algorithms employing the HRC discriminator and of the Julien&al. method, as a function of CNR, upper plots: RMSE, lower plots: MTLL. HRC and SCM HRC curves are overlapping; DC HRC and DC SCM HRC curves are also overlapping (differences at the 4th decimal).

comparison, the performance of introduced feedback techniques is evaluated separately from that of the feedforward methods. The same modulation types as in Section 5.1 are used here, namely, SinBOC$(1, 1)$ and CosBOC$(10, 5)$ modulations. However, the introduced SCM method can be extended to any sine or cosine BOC-modulation case.

The studied techniques have been investigated under the assumption of indoor or outdoor Rayleigh or Rician multipath profiles (i.e., for indoor channel, the speed mobile is set to $\nu = 3$ km/h, while for outdoor profiles, the mobile speeds

of 25, 45, or 75 km/h have been selected). Two main channel profiles have been considered: either with fixed Rayleigh distribution of all paths and with average path power of -1, -2, 0 and -3 dB, or a 2-paths decaying power delay profile (PDP) channel, with Rician distributions for the first path and Rayleigh distribution for the next path. Similar with the AWGN case in Section 5.1, during simulations, the first path delay of the channel is assumed to be linearly increasing, with a slope of 0.05 chips per block of $N_c N_{\text{nc}}$ millisecond, thus the tracking algorithms should capture this linear delay increase. The successive channel path delays have a random spacing with respect to the precedent delay, uniformly distributed between $1/(N_s N_{\text{BOC}_1} N_{\text{BOC}_2})$ and x_{max}, where x_{max} (in chips) is the maximum separation between successive paths (i.e., for closed-spaced paths scenario, $x_{\text{max}} = 0.1$ chips). In order to have independent and reliable results for each method, the search interval is different for each algorithm. which means that once the lock is lost for one method, this will not affect the other algorithms. The search window has few chips (typically between 4 and 12 chips), depending on the number of paths, the distance between them and on the used BOC-modulation orders. The search window is sliding around the previous delay estimate and if we have erroneous estimates, the lock is lost at some point. For the feedback algorithms (i.e., NEML, HRC, or Julien&al. methods), the search for zero crossing is conditioned by the previous delay estimates. Similar with AWGN case, he coherent integration length is set to $N_c = 20$ milliseconds, the noncoherent integration is performed over $N_{\text{nc}} = 3$ blocks, and the oversampling factor is set to $N_s = 11$.

The SCM approach is exemplified in Figure 18, for a Rayleigh 2-paths fading channel, with equal PDP. The upper plot exemplifies a SinBOC$(1, 1)$ modulation case, with $x_{\text{max}} = 1$ chip, while the lower plot shows the original ACF, together with subtracted pulse and unambiguous shape, for a SinBOC$(10, 5)$ case and $x_{\text{max}} = 0.5$ chips. In both cases the threat of the sidelobes is eliminated using the SCM technique. For instance, in the SinBOC$(1, 1)$ case, the correct delay of first path, situated at the 70th sample (in one chip, there are $N_s N_{\text{BOC}_1} N_{\text{BOC}_2}$ samples) is more likely to be detected, after the main sidelobe (situated at the 81th sample) is removed by subtraction.

Figure 19 presents the RMSE and MTLL, for the feedback algorithms which use the NEML discriminator, with an early late spacing of $\Delta = 0.1$ chips. The signal is SinBOC$(1, 1)$ modulated. Here, the Julien&al. method employs an EMLP discriminator, as presented in Section 3.5. The channel is 4-path outdoor Rayleigh channel, $\nu = 75$ km/h, with the most challenging situation of closely-spaced paths (i.e., $x_{\text{max}} = 0.1$ chips). From both plots, it can be seen that both SCM-enhanced methods (the SCM NEML and SCM DC NEML) are performing much better than the other algorithms. Also, the Julien&al. EMLP technique brings an improvement in the results, comparing with both NEML and DC NEML methods, but still not approaching the performance of the SCM algorithms.

Figures 20 and 21 illustrate the performances of the introduced methods using an HRC discriminator. The
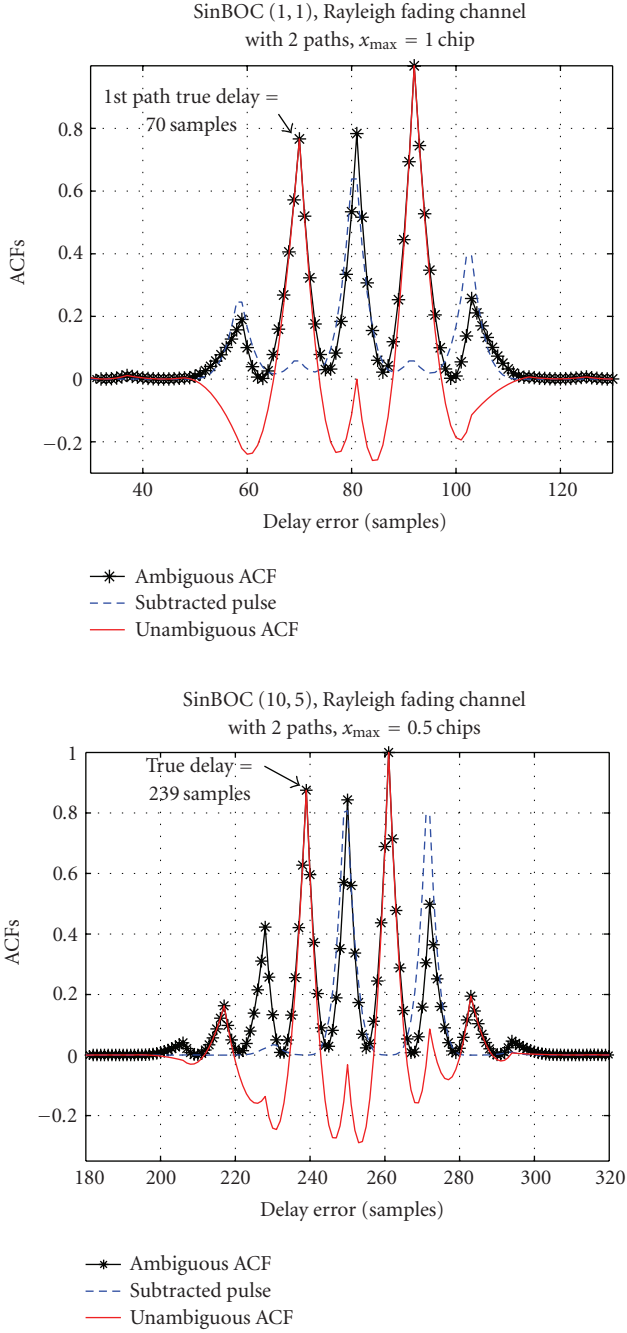
SinBOC$(1, 1)$, Rayleigh fading channel
with 2 paths, $x_{max} = 1$ chip

1st path true delay =
70 samples

— * — Ambiguous ACF
— – – Subtracted pulse
——— Unambiguous ACF

SinBOC$(10, 5)$, Rayleigh fading channel
with 2 paths, $x_{max} = 0.5$ chips

True delay =
239 samples

— * — Ambiguous ACF
— – – Subtracted pulse
——— Unambiguous ACF

FIGURE 18: Exemplification of SCM method for a 2-paths Rayleigh fading channel. Upper plot: SinBOC$(1, 1)$-modulated signal and $x_{max} = 1$ chip. Lower plot: SinBOC$(10, 5)$-modulated signal and $x_{max} = 0.5$ chips.

SinBOC$(1, 1)$, Rayleigh channel,
speed mobile = 75 km/h, $x_{max} = 0.1$ chips

— * — NEML   — □ — DC NEML
— ⊖ — Julien & al. EMLP   — ▷ — SCM DC NEML
— × — SCM NEML

SinBOC$(1, 1)$, Rayleigh channel, 4 paths, $x_{max} = 0.1$ chips

— * — NEML   — □ — DC NEML
— ⊖ — Julien & al. EMLP   — ▷ — SCM DC NEML
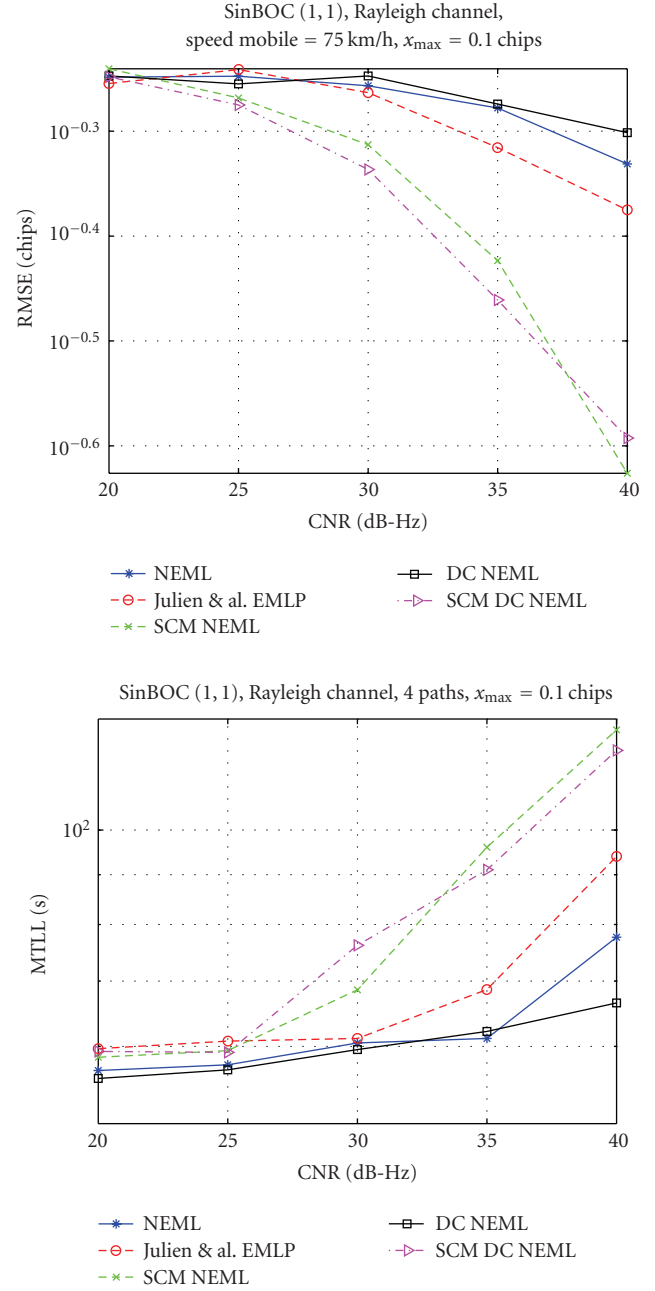— × — SCM NEML

FIGURE 19: Comparison of feedback delays estimation algorithms employing the NEML discriminator and of the Julien&al. method, as a function of CNR; SinBOC$(1, 1)$ modulation, Rayleigh channel with an average pathspower delay profile of -1, -2, 0, and -3 dB, $v = 75$ km/h, closely spaced paths with $x_{max} = 0.1$ chips.

Julien&al. method employs a DP discriminator, as explained in Section 3.5. This selection is done because it has been observed by simulations that the Julien&al. method employing a DP discriminator exceeds the performance of the EMLP discriminator; this behavior is expected since the DP approach does not vary linearly with the code tracking error [20] as the EMLP discriminator. In Figure 20, the signal is SinBOC$(1, 1)$-modulated, for a 2-path channel with Rician

distribution for the first path, a mobile speed of 25 km/h and a large separation between successive paths $x_{max} = 1$ chip. Figure 21 presents the case of a CosBOC$(10, 5)$-modulated signal, for a 4-paths Rayleigh channel, with closely spaced paths $x_{max} = 0.1$ chips and $v = 45$ km/h.

From all plots of Figures 20 and 21, it can be observed that, in both RMSE and MTLL terms, there is a small improvement brought by the DC HRC and SCM DC

SinBOC $(1, 1)$, 2-paths Rician channel,
$x_{max} = 1$ chip, mobile speed $= 25$ km/h

CosBOC $(10, 5)$, Rayleigh channel,
$x_{max} = 0.1$ chips, mobile speed $= 45$ km/h

SinBOC $(1, 1)$, 2-paths Rician channel,
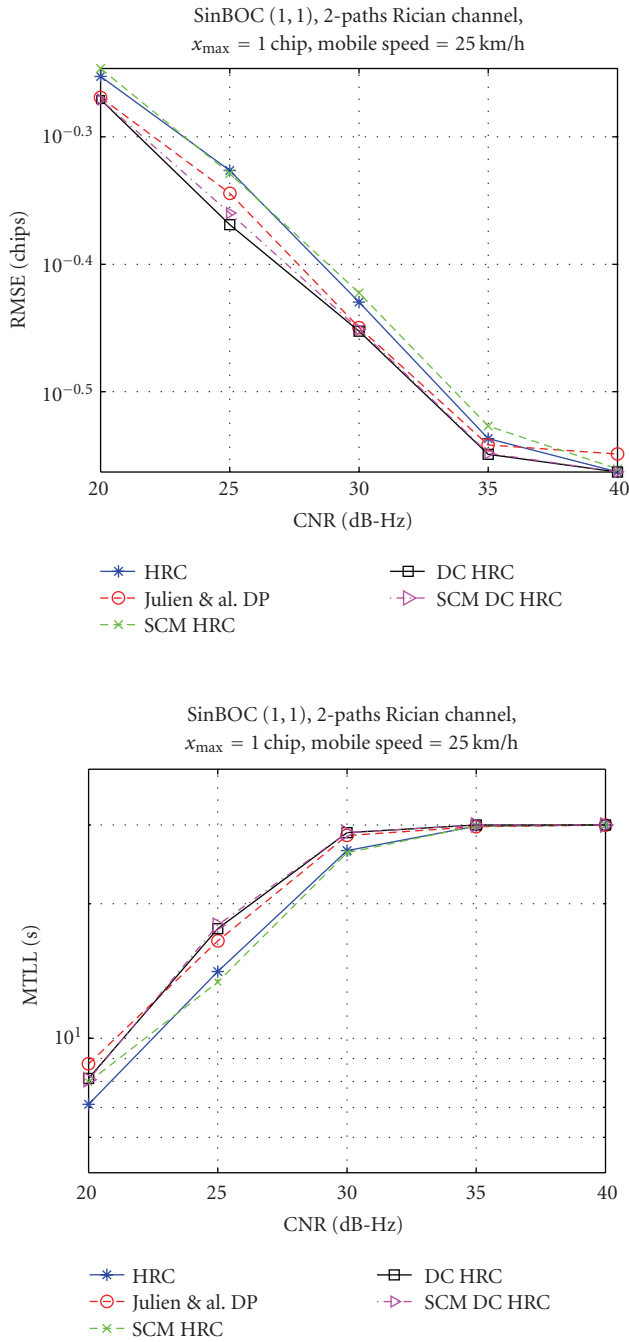$x_{max} = 1$ chip, mobile speed $= 25$ km/h

FIGURE 20: Comparison of feedback delays estimation algorithms employing the HRC discriminator and of the Julien&al. method, as a function of CNR; SinBOC$(1, 1)$ modulation, 2-paths Rician channel with decaying PDP of 0 and -2 dB, $v = 25$ km/h, maximum separation between paths $x_{max} = 1$ chip.

CosBOC $(10, 5)$, 4-paths Rayleigh channel,
$x_{max} = 0.1$ chips

FIGURE 21: Comparison of feedback delays estimation algorithms employing the HRC discriminator and of the Julien&al. method, as a function of CNR; CosBOC$(10, 5)$ modulation, 4-paths Rayleigh channel, with paths PDP of -1, -2, 0, and -3 dB, $v = 45$ km/h, closely spaced paths $x_{max} = 0.1$ chips.

HRC methods, which have similar performance. For the SinBOC$(1, 1)$ case, the performance of the Julien& al. DP method exceeds those of HRC and SCM HRC algorithms, which both give similar results. On the other hand, for the CosBOC$(10, 5)$ modulation, the Julien& al. DP method approaches the results provided by the HRC and SCM HRC algorithms, which still offer a deterioration in performance
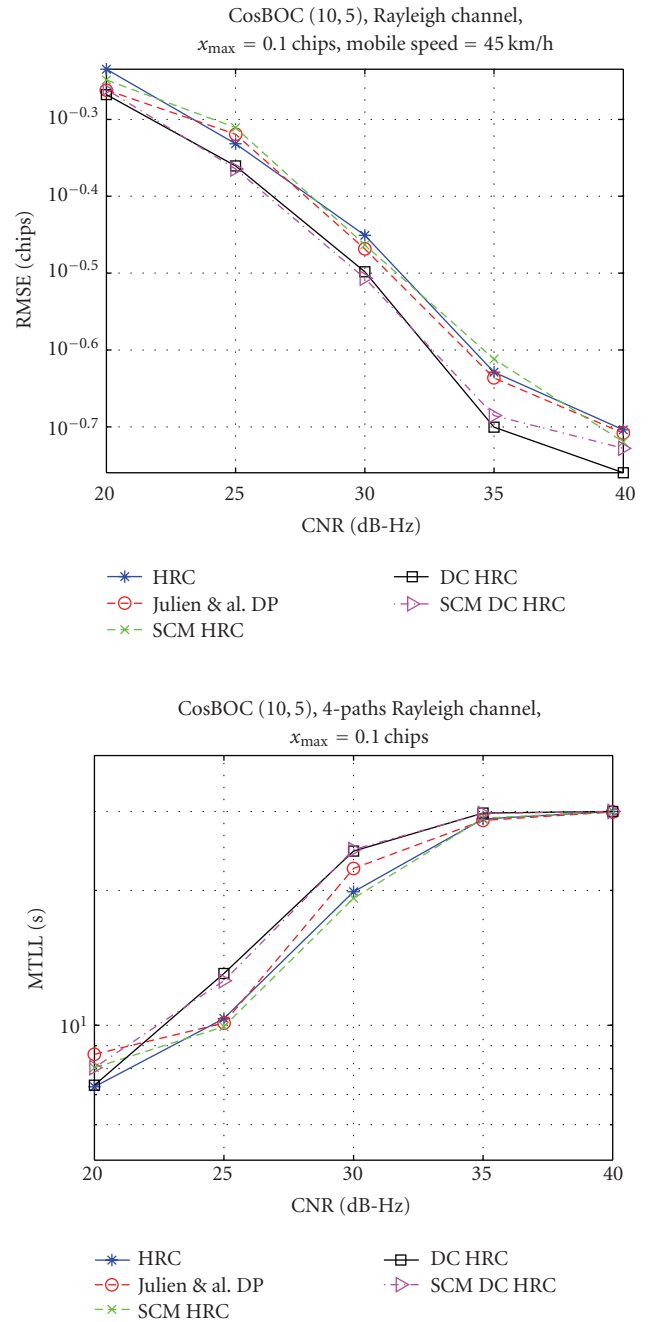
of about 1 dB, comparing to DC HRC and SCM DC HRC methods.

The comparisons between the introduced feedforward delay estimation algorithms (the MEDLL method, the IC enhanced techniques and the SCM with threshold comparison approach) are presented in Figures 22 to 25. In Figure 22, the signal is SinBOC$(1, 1)$-modulated, with a indoor closely
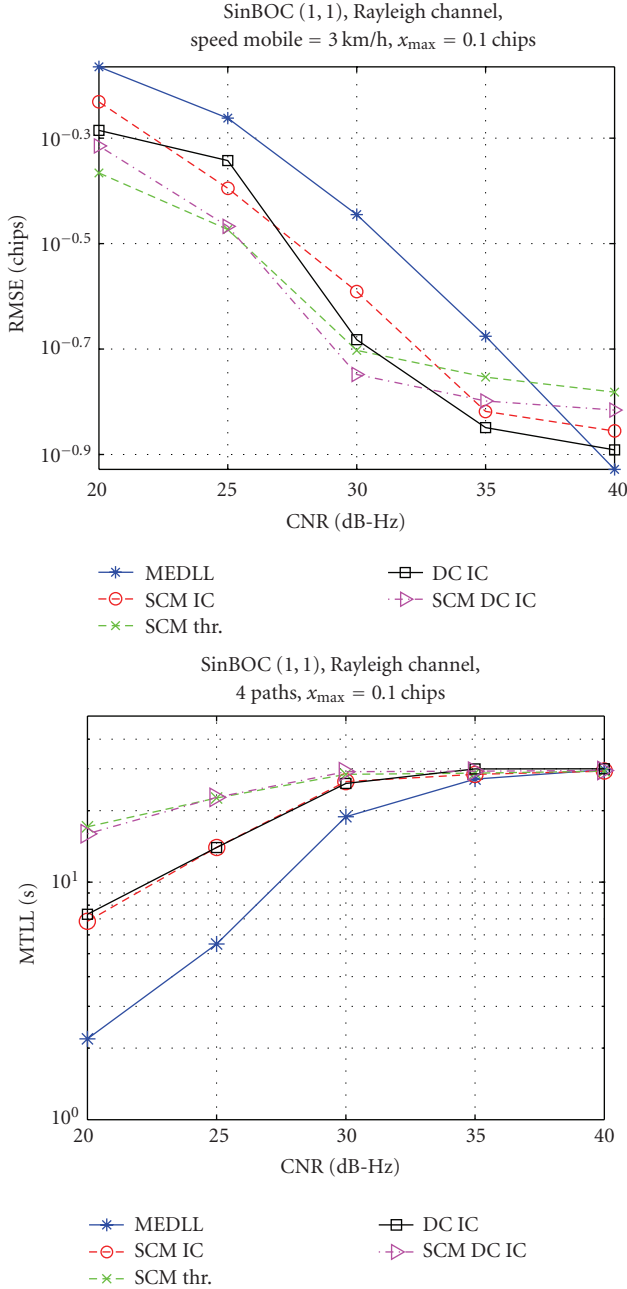
FIGURE 22: Comparison of feedforward delays estimation algorithms employing the MEDLL and IC methods and of the SCM with threshold approach, as a function of CNR; SinBOC(1, 1) modulation, 4-paths indoor Rayleigh channel, with PDP of -1, -2, 0, and -3 dB, $v = 3$ km/h, closely spaced paths with $x_{max} = 0.1$ chips.
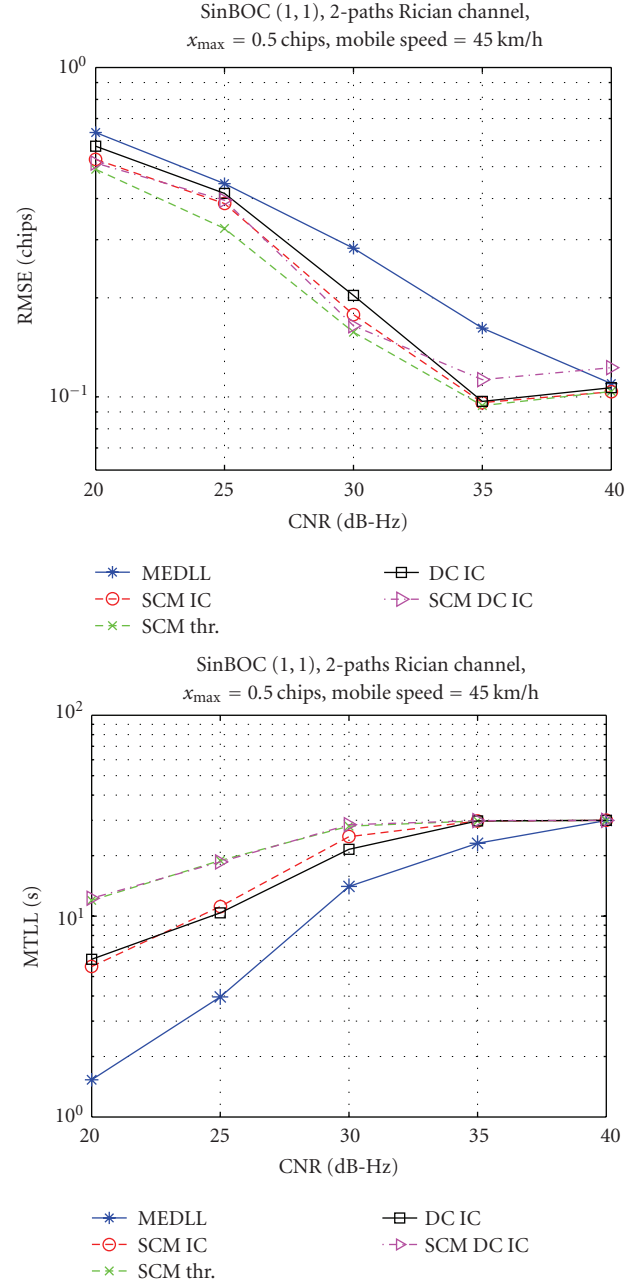
FIGURE 23: Comparison of feedforward delays estimation algorithms employing the MEDLL and IC methods and of the SCM with threshold approach, as a function of CNR; SinBOC(1, 1) modulation, 2-paths decaying PDP Rician channel, $v = 45$ km/h, $x_{max} = 0.5$ chips.

spaced paths Rayleigh channel ($x_{max} = 0.1$ chips, $v = 3$ km/h). In Figure 23, the signal is also SinBOC(1, 1) modulated, the channel is 2-paths with Rician distribution on first path, $v = 45$ km/h and $x_{max} = 0.5$ chips.

In all plots the performance of MEDLL algorithm is exceeded by the other methods, since they eliminate or decrease the threats of the sidelobes. In terms of RMSE, for a Rayleigh profile with closely-spaced paths (Figure 22, upper plot), the performances of the SCM IC and DC IC algorithms

are exceeded by those of SCM DC IC and SCM thresholding methods, for a CNR range from 20 to 30 dB-Hz. In case of Figure 23, for a higher spacing between successive paths up to 0.5 chips and a higher mobile speed, the SCM with threshold comparison gives the best results, while the SCM IC and SCM DC IC methods have similar performance, which is still better then that of DC IC, for a range of about 20 to 33 dB-Hz.

In terms of MTLL, from both Figure 22 and Figure 23, lower plots, can be concluded that the best performance
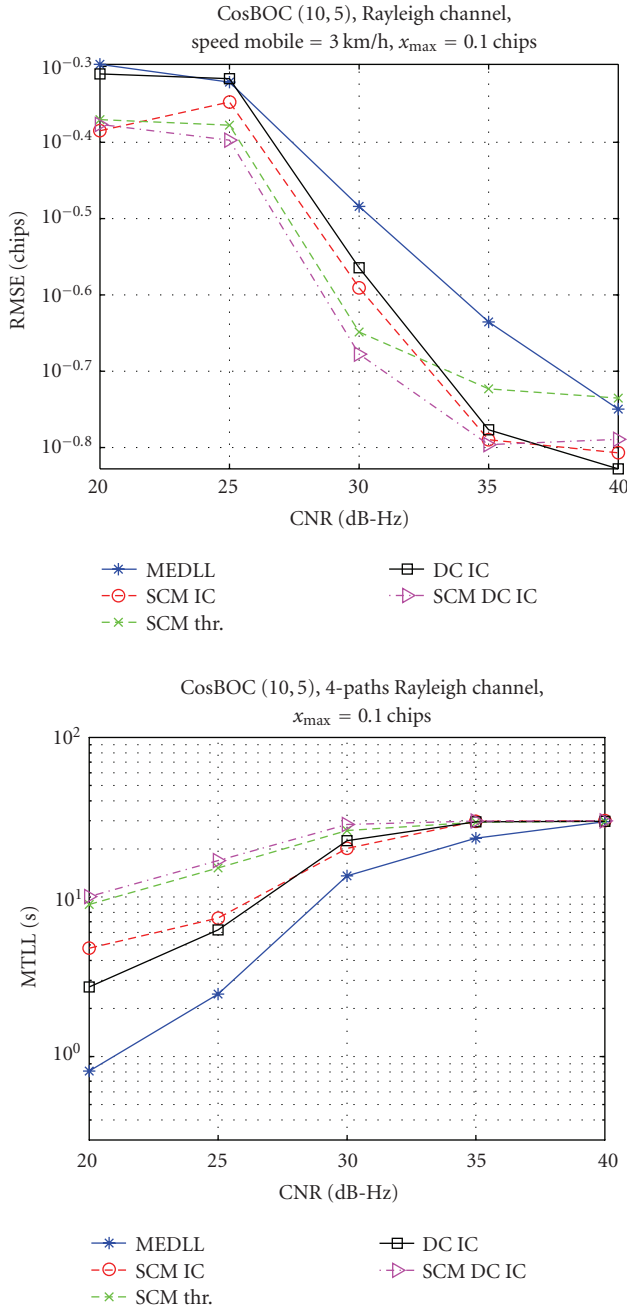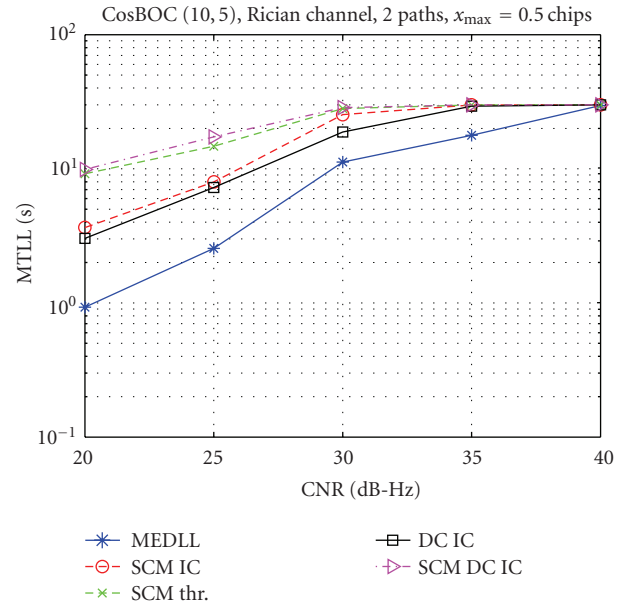
FIGURE 25: Comparison of feedforward delays estimation algorithms employing the MEDLL and IC methods and of the SCM with threshold approach, as a function of CNR; CosBOC(10, 5) modulation, 2-paths decaying PDP Rician channel, $v = 45$ km/h, $x_{max} = 0.5$ chips.

upper plot), the SCM DC IC method gives the best results, followed by the SCM with threshold comparison and SCM IC methods, for a CNR range of up to 33 dB-Hz. The good performance of SCM DC IC method is expected, since for a higher BOC-modulation order, it eliminates more sidelobes than the other SCM methods (as illustrated in Figure 15). The MEDLL technique is still outperformed by all the other methods.

In terms of MTLL (Figure 24, lower and plot and Figure 25), for both channel profile cases, the SCM with threshold comparison and SCM DC IC approaches have the best performance, while the SCM IC technique brings an improvement over the DC IC case (in contrast with the SinBOC(1, 1) situation, i.e., Figure 22). This is explicable, since the SCM approach removes completely the sidelobes situated near the main peak, while the DC method just decreases their amplitudes (Figure 15).

Figure 26 presents the effect of maximum separation between successive paths x_{max}, in case of feedback delay estimation algorithms which use NEML discriminator, together with the Julien&al. EMLP method. The channel has a 4-paths indoor Rayleigh profile with the mobile speed of 4 km/h and the CNR is set to 35 dB-Hz. In this case, both SCM algorithms provide a decreasing in error as x_{max} is increasing, while the other methods have an almost linear behavior, for x_{max} greater than half of chip. Also, it can be observed that the same gap between the studied methods, at $x_{max} = 0.1$ chips, is presented in Figure 19, upper plot.

6. CONCLUSIONS

A new tracking technique (the sidelobes cancellation method) has been introduced, which removes or diminishes

FIGURE 24: Comparison of feedforward delays estimation algorithms employing the MEDLL and IC methods and of the SCM with threshold approach, as a function of CNR; CosBOC(10, 5) modulation, 4-paths indoor Rayleigh channel, $v = 3$ km/h, closely-spaced paths $x_{max} = 0.1$ chips.

(i.e., the highest MTLL) is provided by the SCM DC IC and SCM thresholding algorithms, with an improvement of about 4-5 dB-Hz comparing to SCM IC and DC IC methods, which give similar results.

Figures 24 and 25 illustrate the obtained simulation results, for a CosBOC(10, 5)-modulated signals, for a 4-closely-spaced paths indoor Rayleigh profile, respectively for a 2-paths channel, with $v = 45$ km/h and a separation between paths x_{max} of up to 0.5 chips. In terms of RMSE (Figure 24,

SinBOC $(1, 1)$, 4-paths Rayleigh channel,
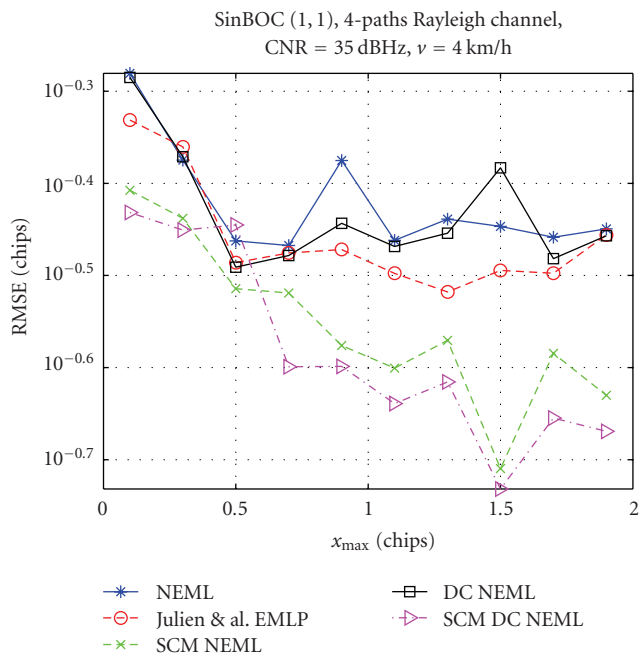CNR = 35 dBHz, $v = 4$ km/h

FIGURE 26: Comparison of feedback delays estimation algorithms employing the NEML discriminator and of the Julien&al. EMLP method, as a function of separation between successive channel paths xmax, in terms of RMSE; SinBOC$(1, 1)$ modulation, 4-paths Rayleigh channel, mobile speed 4 km/h, CNR = 35 dB-Hz.

the sidelobes ambiguities of the BOC-modulated signals, while keeping the narrow width of the main lobe, which is benefic for the tracking process. In contrast with other methods, this algorithm has the advantage that can be applied to any sine or cosine, odd or even BOC-modulation case. It also provides a lower complexity solution, since it uses ideal reference correlation functions, which are generated only once and can be stored at receiver side. The performance of the SCM algorithm can be enhanced if other tracking-loop methods are used after removing the sidelobes and the multipath problem can be alleviated, since the undesired effect of short delay multipath can be reduced. It has been shown through extensive simulation results, that in case of multipath fading channels, with both closely spaced or long delayed paths, the introduced SCM algorithms bring an improvement in performance compared to other considered delay tracking methods. The highest performance improvement comes when combining SCM technique with the narrow EML correlator. The combination between HRC and SCM does not bring substantial improvement, since HRC has already rather good performance in multipath channels. Also, the higher BOC-modulation order, the more advantageous is to apply SCM technique in order to cope better with the false lock points.

ACKNOWLEDGMENTS

REFERENCES

[1] J. Betz and D. Goldstein, "Candidate designs for an additional civil signal in GPS spectral bands," Tech. Rep., MITRE, Bedford, Mass, USA, 2002. http://www.mitre.org/work/tech_papers/tech_papers_02/betz_candidate/.

[2] B. Barker, J. Betz, J. Clark, et al., "Overview of the GPS M code signal," in *CDROM Proceedings of the ION National Meeting; Navigating into the New Millennium*, Anaheim, Calif, USA, January 2000.

[3] GJU, "Galileo Open Service—Signal in Space Interface Control Document (OS SIS ICD)," Galileo Joint Undertalikng (GJU), http://www.galileoju.com/, May 2006.

[4] E. S. Lohan, A. Lakhzouri, and M. Renfors, "Feedforward delay estimators in adverse multipath propagation for Galileo and modernized GPS signals," *EURASIP Journal on Applied Signal Processing*, vol. 2006, Article ID 50971, 19 pages, 2006.

[5] J. Betz, "The offset carrier modulation for GPS modernization," in *Proceedings of the National Technical Meeting of the Institute of Navigation (ION-NTM '99)*, pp. 639–648, San Diego, Calif, USA, January 1999.

[6] J. Betz, "Design and performance of code tracking for the GPS M code signal," Tech. Rep., MITRE, Mclean, Va, USA, September 2000, http://www.mitre.org/work/tech_papers/tech_papers_00/betz_codetracking/.

[7] J. Holmes, S. Raghavan, and S. Lazar, "Acquisition and tracking performance of NRZ and square wave modulated symbols for use in GPS," in *Proceedings of the 54th Annual Meeting of the Institue of Navigation*, pp. 611–625, Denver, Colo, USA, June 1998.

[8] A. V. Dierendonck, P. Fenton, and T. Ford, "Theory and performance of narrow correlator spacing in a GPS receiver," *Journal of the Institute of Navigation*, vol. 39, no. 3, pp. 265–283, 1992.

[9] M. Irsigler and B. Eissfeller, "Comparison of multipath mitigation techniques with consideration of future signal structures," in *Proceedings of the International Technical Meeting of the Institute of Navigation (ION-GPS/GNSS '03)*, pp. 2584–2592, Portland, Ore, USA, September 2003.

[10] A. McGraw and M. Braasch, "GNSS multipath mitigation using high resolution correlator concepts," in *Proceedings of the National Technical Meeting of the Institute of Navigation (ION-NTM '99)*, pp. 333–342, San Diego, Calif, USA, January 1999.

[11] L. Garin and J.-M. Rousseau, "Enhanced strobe correlator multipath rejection for code and carrier," in *Proceedings of the 10th International Technical Meeting of the Satellite Division of the Institute of Navigation (ION-GPS '97)*, vol. 1, pp. 559–568, Kansas City, Mo, USA, September 1997.

[12] J. Jones, P. Fenton, and B. Smith, "Theory and performance of the pulse aperture correlator," Tech. Rep., NovAtel, Calgary, Alberta, Canada, September 2004, http://www.novatel.com/Documents/Papers/PAC.pdf.

[13] A. V. Dierendonck and M. Braasch, "Evaluation of GNSS receiver correlation processing techniques for multipath and noise mitigation," in *Proceedings of the National Technical Meeting of the Institute of Navigation (ION-NTM '97)*, pp. 207–215, Santa Monica, Calif, USA, January 1997.

[14] C. Lee, S. Yoo, S. Yoon, and S. Y. Kim, "A novel multipath mitigation scheme based on slope differential of correlator output for Galileo systems," in *Proceedings of the 8th International Conference on Advanced Communication Technology (ICACT '06)*, vol. 2, pp. 1360–1363, Phoenix Park, Korea, February 2006.

[15] R. van Nee, J. Siereveld, P. Fenton, and B. Townsend, "The multipath estimating delay lock loop: approaching theoretical accuracy limits," in *Proceedings of IEEE Position Location and Navigation Symposium*, pp. 246–251, Las Vegas, Nev, USA, April 1994.

[16] P. A. Bello and R. L. Fante, "Code tracking performance for novel unambiguous M-code time discriminators," in *Proceedings of the National Technical Meeting of the Institute of Navigation (ION-NTM '05)*, pp. 293–298, San Diego, Calif, USA, January 2005.

[17] P. Fine and W. Wilson, "Tracking algorithms for GPS offset carrier signals," in *Proceedings of the National Technical Meeting of the Institute of Navigation (ION-NTM '99)*, San Diego, Calif, USA, January 1999.

[18] V. Lin, P. Dafesh, A. Wu, and C. Cahn, "Study of the impact of false lock points in subcarrier modulated ranging signals and recommended mitigation approaches," in *Proceedings of the 59th ION Annual Meeting & CIGTF Guidance Test Symposium*, pp. 156–165, Albuquerque, NM, USA, June 2003.

[19] P. Ward, "A design technique to remove the correlation ambiguity in binary offset carrier (BOC) spread spectrum signals," in *Proceedings of the National Technical Meeting of the Institute of Navigation (ION-NTM '04)*, pp. 886–896, San Diego, Calif, USA, January 2004.

[20] O. Julien, C. Macabiau, M. Cannon, and G. Lachapelle, "BOC signal acquisition and tracking method and apparatus," US Patent Application Publication 2005/0270997 A1, December 2005.

[21] V. Heiries, J.-A. Avila-Rodriguez, M. Irsigler, G. Hein, E. Rebeyrol, and D. Roviras, "Acquisition performance analysis of composite signals for the L1 OS optimized signal," in *Proceedings of the 18th International Technical Meeting of the Satellite Division of the Institue of Navigation (ION-GNSS '05)*, pp. 877–889, Long Beach, Calif, USA, September 2005.

[22] A. Schmid and A. Neubauer, "Differential correlation for Galileo/GPS receivers," in *Proceedings IEEE International Conference on Acoustics, Speech, and Signal Processing (ICASSP '05)*, vol. 3, pp. 953 –956, Philadelphia, Pa, USA, March 2005.

[23] A. Burian, E. S. Lohan, and M. Renfors, "Sidelobe cancellation method for unambiguous tracking of binary-offset-carrier modulated signals," in *CDROM Proceedings of the 3rd ESA Workshop on Satellite Navigation User Equipment Technologies (NAVITEC '06)*, Noordwijk, The Netherlands, December 2006.

[24] G. Hein, J. Godet, J.-L. Issler, J. C. Martin, T. Pratt, and R. Lucas, "Status of Galileo frequency and signal design," in *CDROM Proceedings of the International Technical Meeting of the Satellite Division of the Institute of Navigation (ION-GPS '02)*, Portland, Ore, USA, September 2002.

[25] E. S. Lohan, A. Lakhzouri, and M. Renfors, "Binary-offset-carrier modulation techniques with applications in satellite navigation systems," *Wireless Communications and Mobile Computing*, vol. 7, no. 6, pp. 767–779, 2006.

[26] E. Rebeyrol, C. Macabiau, L. Lestarquit, et al., "BOC power spectrum densities," in *CDROM Proceedings of the National Technical Meeting of Institute of Navigation (ION-NTM '05)*, San Diego, Calif, USA, January 2005.